and Dimmock, 1985; Renegar et al., 1998]. The polymeric nature of S-IgA also explains why S-IgA cross-reacts with variant influenza viruses to a greater extent than serum IgG [Tamura et al., 1990, 1991, 1992; Asahi-Ozaki et al., 2004]. Thus, intranasal administration of an inactivated influenza vaccine is advocated to elicit S-IgA and IgG responses and improve the protective efficacy of current vaccination procedures [Tamura and Kurata, 2004; Tamura et al., 2005, 2010].

Several clinical trials have examined the induction of both S-IgA and IgG following intranasal administration of inactivated influenza vaccines, either with or without adjuvant [Kuno-Sakai et al., 1994; Hashigucci et al., 1996; Muszkat et al., 2000; Greenbaum et al., 2002; Durrer et al., 2003; Treanor et al., 2006; Atmar et al., 2007]. The antibody responses after intranasal administration of inactivated influenza vaccines were assessed by measuring hemagglutination inhibition (HI) titres in the serum, and anti-hemagglutinin (HA) IgA and IgG titres in nasal wash samples. They did not measure the titre of neutralizing antibodies, which is considered to be a better criterion for functional protective antibodies. Neutralization titres can directly inhibit the complex process involved in virus replication, which include virus attachment and entry to the host cells, and release of newly-synthesized virus from the infected cells in tissue culture. In addition, a previous study found that HI titres were lower, or higher, than the corresponding neutralization titres, depending on a strain of influenza A or B virus used for the assay [Okuno et al., 1990], whereas other studies show that anti-H5 HI antibodies fail to detect H5N1 viruses [Lu et al., 1982; Rowe et al., 1999]. Thus, neutralizing antibody responses following intranasal administration of an inactivated influenza vaccine remain to be fully characterized.

Therefore, the aim of the present study was to examine the levels and properties of neutralizing-antibodies in nasal wash and serum samples from healthy adults after intranasal administration of an inactivated vaccine (five doses, with an interval of 3 weeks between each dose). The inactivated vaccine used in this study was a concentrated split-virus vaccine (containing 45 μg HA per dose), prepared from the A/Uruguay/716/2007 (H3N2) strain. A concentrated split-virus vaccine was chosen because the vaccine has already been shown to induce mucosal antibody responses after intranasal vaccination [Kuno-Sakai et al., 1994]. To ensure that neutralization titres specific for the A/Uruguay/716/2007 virus were assayed at equivalent levels in both serum and nasal wash samples, the neutralization titres were measured using concentrated nasal wash samples (1 mg/ml total protein) that contained approximately 1/10 of the IgA found in undiluted mucus [Kurono and Mogi, 1987]. The properties of the neutralizing IgA and IgG antibodies induced by intranasal vaccination were then examined, and their relative levels and molecular size were determined.

## MATERIALS AND METHODS

### Subjects

Five healthy male subjects (P1, P2, P3, P4, and P5) were enrolled in the study (aged 22, 32, 42, 42, and 68 years, respectively, at the time of the first vaccination). All participants had already acquired some degree of immunity to H1N1 and H3N2 influenza A virus subtypes after previous exposure to these viruses and/or as a result of previous vaccinations. Each subject provided informed consent and the study protocol and other relevant documentation were reviewed and approved by the Ethics Committee of the National Institute of Infectious Diseases (Tokyo, Japan).

### Virus and Vaccine

The A/Uruguay/716/2007 (A/Uruguay; H3N2) influenza virus strain was propagated in the allantoic cavity of 10-day-old embryonated hen's eggs and purified from the allantoic fluid. The $TCID_{50}$ (50% infectious dose in tissue culture) of the virus was estimated as described previously [Tobita et al., 1975; Kadowaki et al., 2000]. In brief, 10-fold serial dilutions of the allantoic fluid containing the virus were inoculated into Madin-Darby canine kidney (MDCK) cells (ATCC No. CCL-34) cells in 96-well culture plates and incubated for 4 days at 37°C in a 5% $CO_2$ humidified atmosphere. The cytopathic effects in the virus-containing wells were monitored under a microscope and the $TCID_{50}$ was calculated using the Reed–Muench method. The split product virus vaccine was supplied by the Research Foundation for Microbial Disease of Osaka University (BIKEN, Kanonji, Japan). The vaccine was prepared from purified viruses, which were sedimented through a linear sucrose gradient according to the manufacturer's protocol. The viruses were then treated with ether and formalin according to the manufacturer's protocol, which was based on the method of Davenport et al. [1964]. The concentrated split vaccine containing 45 μg HA was the product of a process used to prepare a trivalent vaccine comprising A/H1N1, A/H3N2, and B type vaccines, each containing 15 μg HA.

### Vaccinations

All participants were immunized intranasally with a threefold concentrated split H3N2 virus vaccine (A/Uruguay, containing 45 μg HA). Each received five doses, with an interval of 3 weeks between each dose. Intranasal vaccination was performed by spraying 0.25 ml of the split vaccine into each nostril (0.5 ml total) using an atomizer (Keytron, Ichikawa, Japan). The mean droplet diameter was 56.5 μm, ranging in size between 10 μm and 90 μm.

### Nasal Wash and Serum Samples

About 100 ml of nasal wash was collected from each participant in polypropylene tubes by washing the

nasal cavity several times using a nose irrigation device (Hananoa; Kobayashi Pharmaceutical, Osaka, Japan) filled with saline solution according to the manufacturer's instructions. Pieces of dental cotton (Dental Cotton Roll; B.S.A. Sakurai, Nagoya, Japan) were then immersed in the collected nasal washes. Dental cotton pieces (containing a combined absorbed volume of about 25 ml of nasal wash) were then placed into a filter insert (Oxi Fil filter insert; TOHO, Tokyo, Japan) with bottoms drilled to create several pores, and placed in 50 ml polypropylene centrifuge tubes. Clean nasal wash was separated from mucopolysaccharides and other debris by centrifugation at 2,200*g* for 5 min at room temperature. This procedure was repeated for the entire 100 ml nasal wash sample from each participant. The pooled, clean nasal wash was then concentrated to a final volume of approximately 0.5 ml using Vivaspin centrifugal concentrators (Vivaspin 20, MWCO = 30,000; Sartorius Stedim Biotech, Aubagne, France). The concentrated nasal wash was stored at −80°C before use.

### Quantitation of IgA, IgG and IgM Antibodies and Other Proteins

The levels of human IgA, IgG, and IgM antibodies in the nasal wash and serum samples were estimated using human IgA, IgG, or IgM ELISA kits (Bethyl Laboratories, Montgomery, USA). The level of human serum albumin in the nasal wash samples was estimated using a Human Albumin ELISA kit (Bethyl Laboratories). The protein concentration in the samples was measured using either a BCA Protein Assay Kit, or a Micro BCA Protein Assay Kit (Thermo Fisher Scientific, Yokohama, Japan) according to the manufacturer's instructions.

### Neutralization Assays

The level of serum antibodies against the vaccine viruses was examined using micro-neutralization assays as previously described [Belshe et al., 2000; Kadowaki et al., 2000] with minor modifications. In brief, serum samples were treated with a receptor-destroying enzyme (RDE(II); Denka Seiken, Tokyo, Japan) overnight at 37°C and heat-inactivated for 30 min at 56°C before use. The first dilution tested in the assays was 1:10. The concentrated nasal wash samples [1 mg/ml total protein, corresponding to about 1/10 of the total IgA found in nasal mucus (2.20 mg/ml)] [Kurono and Mogi, 1987] were also treated with RDE(II) and heat-inactivated before use. The first dilution tested in the nasal wash assays was 1:20. Twofold serial dilutions of the serum samples were mixed with an equal volume (50 μl) of diluent containing influenza virus equivalent to 100 $TCID_{50}$. Each mixture was added to the wells of a 96-well plate containing a monolayer of MDCK cells. Four control wells were included on each plate and contained either virus or diluent alone. The plates were then incubated for 4 days at 37°C in a 5% $CO_2$-humidified atmosphere. The monolayer in each well was observed for the presence or absence of cytopathic effects, fixed with 10% formalin for more than 5 min at room temperature, and stained with Naphthol blue black. After the plates were washed and dried, the stained cells were solubilized with 0.1 M NaOH and the absorbance (A) was measured at 630 nm. The average $A_{630\ nm}$ value was determined from quadruplicate virus-infected wells ($A_{virus}$) and cell culture-only controls ($A_{cell}$). All values above 50% of the specific signal, calculated using the formula: $X = (1/2) \times (A_{cell} - A_{virus}) + A_{virus}$, were considered positive for neutralization. The titres recorded were the reciprocal of the highest dilution, where $A_{630}$ was >X.

### Hemagglutination Inhibition

The antibody responses to the vaccine viruses were examined in serum and nasal washes using HI antibody assays incorporating a microtiter method as described elsewhere [Hierholzer et al., 1969]. All samples were pre-treated with RDE(II) at 37°C for 18 hr, subsequently inactivated at 56°C for 30 min, and mixed with packed red blood cells to remove any nonspecific inhibitors. The starting material for the assays was a 1:10 dilution for the serum samples and a 1:40 dilution for the nasal wash samples.

### Fractionation of Nasal and Serum Samples

The concentrated nasal wash samples (100 μl, 6 mg/ml) and diluted serum samples (10-fold dilution, 100 μl, about 6 mg/ml) were fractionated on a Superose 6 10/300 GL gel filtration column using an FPLC-AKTA chromatography system (GE Healthcare, Little Chalfont, UK). The concentrated nasal wash sample was treated with 1 μg/ml of lysozyme (Sigma-Aldrich, St. Louis, MO) for 1 hr at 37°C to decrease the viscosity and then centrifuged using Vivaspin to remove the lysozyme prior to gel filtration. Fractions (each 500 μl) were collected in PBS at a flow rate of 0.1 ml/min; little or no change in the fractionation pattern of the antibodies in the concentrated nasal wash samples was observed following lysozyme treatment. Molecular weight marker proteins (Kit for Molecular Weights 29,000–700,000 Da; Sigma-Aldrich) were eluted under the same conditions to determine the size of each fraction.

## RESULTS

### Measurement of Neutralization and HI Titres in Concentrated Nasal Wash Samples

The total protein level and the levels of IgA, IgG, and IgM and human serum albumin in 100 ml of unconcentrated nasal wash and in approximately 0.5 ml of concentrated nasal wash are shown in Table I. About 70% of the total nasal wash proteins were lost during the concentration process. Also, a fraction of the higher molecular weight (MW) proteins and lower MW proteins (less than 30 kDa) was lost by

TABLE I. Concentration of IgA, IgG, IgM and HSA in 0.5 ml of Solution Concentrated From 100 ml of Nasal Wash (n = 10)*

| Unit | Concentration: Mean ± SD | | | | |
|---|---|---|---|---|---|
| | Total protein | IgA | IgG | IgM | HSA |
| Nasal wash (n = 10) | | | | | |
| Unconcentrated mg/100 ml | 5.875 ± 1.856 | 1.132 ± 0.678 | 0.125 ± 0.057 | 0.032 ± 0.021 | 0.531 ± 0.280 |
| Concentrated mg/0.43 ± 0.06 ml | 1.647 ± 0.549 | 0.375 ± 0.193 | 0.093 ± 0.044 | 0.007 ± 0.006 | 0.292 ± 0.214 |
| Concentration calculated in terms of total protein (mg/ml) | 1.00 | 0.217 | 0.057 | 0.004 | 0.177 |

*The concentration was calculated using two nasal wash samples collected from five participants (with a 1 week interval).

adsorption to the cotton and during Vivaspin centrifugation, respectively. However, better recovery was observed for IgA and IgG. When the concentration of the enriched nasal washes was adjusted to 1 mg/ml total protein, the amount of IgA was 0.217 mg/ml. This amount of IgA in the concentrated nasal wash corresponded to about 1/10 of the levels of total IgA recovered from nasal mucus (2.20 mg/ml) by aspiration as reported by Kurono and Mogi [1987] (Table I). In subsequent experiments, neutralization and HI titres in the nasal wash samples were measured using concentrated nasal wash proteins (1 mg/ml of total protein), which contained 1/10 of the IgA found in mucus, to ensure that the nasal and serum neutralization titres were assayed at equivalent levels.

The amount of total IgA and total IgG in the nasal wash samples from each participant varied slightly at each sampling time. Also, the level of total IgA and IgG antibodies did not increase significantly between pre-vaccination and post-vaccination in any of the participants. Thus, the average amount of total IgA or total IgG in the nasal wash samples from the five participants was relatively constant (data not shown).

## Neutralizing Antibody Responses in Nasal Wash and Serum Samples

Next, antibody responses in the nasal wash and serum samples were examined in all five study participants. The responses are presented as neutralization titres against the A/Uruguay (H3N2) virus in Table II. The responses recorded in the four young adults (between 18- and 50-years-old) are also shown as geometric neutralization titres (Fig. 1). The nasal wash and serum neutralization titres increased in all participants as the number of vaccinations increased, although the degree of increase differed between participants. In addition, nasal wash neutralization titres increased more rapidly than serum titres. The nasal wash titres showed at least a fourfold increase after the second vaccination in the four young participants (all of whom had a nasal wash neutralization titre of 1:20 or 1:40 before vaccination). By contrast, a fourfold increase in the serum titre was observed only after the fifth vaccination in three of the participants (all of whom had serum titres of <1:10, 1:20, or 1:40 before vaccination). Participant P5, who was 67 years old, showed at least a fourfold increase in nasal wash titre after the fourth vaccination, but no significant

TABLE II. Neutralizing Antibody Responses in Subjects who Received the Threefold Concentrated A/Uruguay/716/2007 (H3N2) Split Vaccine

| | Neutralization titre against A/Uruguay virus (H3N2)[a] | | | | | | | | | |
|---|---|---|---|---|---|---|---|---|---|---|
| | P1 | | P2 | | P3 | | P4 | | P5 | |
| Weeks (vaccination) | Nasal wash | Serum | Nasal wash | Serum | Nasal wash | Serum | Nasal wash | Serum | Nasal wash | Serum |
| 0 (1st) | 20 (1) | 40 (2) | 20 (1) | <10 (<0) | 40 (2) | 20 (1) | 20 (1) | <10 (<0) | 20 (1) | <10 (<0) |
| 3 (2nd) | 80 (3) | 160 (4) | 20 (1) | <10 (<0) | 80 (3) | 20 (1) | 20 (1) | <10 (<0) | 40 (2) | <10 (<0) |
| 6 (3rd) | 160 (4) | 160 (4) | 80 (3) | 10 (0) | 320 (5) | 20 (1) | 80 (3) | <10 (<0) | 40 (2) | <10 (<0) |
| 9 (4th) | 320 (5) | 160 (4) | 160 (4) | 20 (1) | 1280 (7) | 40 (2) | 160 (4) | 10 (0) | 40 (2) | <10 (<0) |
| 12 (5th) | 320 (5) | 160 (4) | 320 (5) | 40 (2) | 2560 (8) | 80 (3) | 80 (3) | 10 (0) | 80 (3) | <10 (<0) |
| 15 | 1280 (7) | 160 (4) | 320 (5) | 40 (2) | 2560 (8) | 80 (3) | 160 (4) | 20 (1) | 160 (4) | 10 (0) |
| 28 | 640 (6) | 160 (4) | 160 (4) | 40 (2) | 1280 (7) | 80 (3) | N.D. | N.D. | 80 (3) | 10 (0) |

N.D., not done.
[a]Respective values are a reciprocal titre and a geometric titre ($10 \times 2^n$) in a parenthesis.

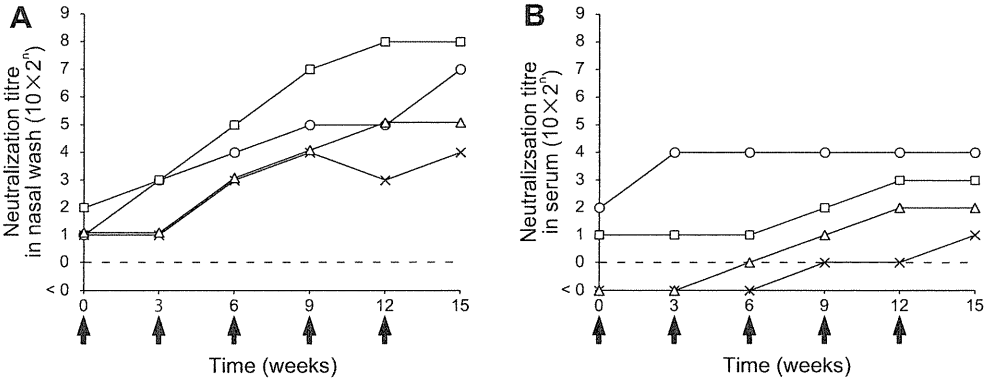


Fig. 1. Nasal wash and serum sample neutralization titres against A/Uruguay (H3N2) (pre- and post-intranasal immunization). Neutralization titres against the A/Uruguay virus in nasal washes (**A**) and serum (**B**) were determined in samples collected from four participants (18–60 years old; P1, open circle; P2, open triangle; P3, open square; and P4, cross). The participants were given five doses of the threefold concentrated A/Uruguay split influenza vaccine intranasally with an interval of 3 weeks between doses (each arrow indicates a point of vaccination). The neutralization titre shown is the geometric titre.

increase was observed in serum titre after five vaccinations. In all participants, the nasal wash and serum titres were largely maintained, even at 16 weeks after the fifth vaccination, at which point the nasal wash titre decreased only slightly, while no decrease was observed in the serum titre (Table II).

## HI Antibody Responses in Nasal Wash and Serum Samples

Antibody responses were also examined by measuring the HI titre against the A/Uruguay (H3N2) virus. Table III shows the pre-vaccination HI titres of the nasal wash and serum samples from two participants, and the HI titres 3 weeks after each of the five vaccinations. For each participant, the HI titres were lower than the neutralization titres shown in Table II. The HI titres were approximately 1/4–1/8 the level of the neutralization titres. Statistical correlation analysis of the data presented in Tables II and III showed a strong correlation between the HI titres and the neutralization titres ($r = 0.8699$). Thus, the HI titre correlated with the neutralization titre, although it was less sensitive than the neutralization titre.

TABLE III. Hemagglutinin Inhibition (HI) Antibody Responses in Subjects who Received the Threefold Concentrated A/Uruguay/716/2007 (H3N2) Split Vaccine

| | HI titre against A/Uruguay virus (H3N2)[a] | | | |
|---|---|---|---|---|
| | P1 | | P2 | |
| Weeks (vaccination) | Nasal wash | Serum | Nasal wash | Serum |
| 0 (1st) | N.D. | 10 (0) | <40 (<2) | <10 (<0) |
| 3 (2nd) | <40 (<2) | 20 (1) | <40 (<2) | <10 (<0) |
| 6 (3rd) | <40 (<2) | 20 (1) | <40 (<2) | <10 (<0) |
| 9 (4th) | 40 (2) | 20 (1) | <40 (<2) | 10 (0) |
| 12 (5th) | 40 (2) | 20 (1) | 80 (3) | 20 (1) |
| 15 | 160 (4) | 40 (2) | 80 (3) | 20 (1) |

N.D., not done.
[a]Respective values are a reciprocal titre and a geometric titre ($10 \times 2^n$) in a parenthesis.

## Fractionation of The Nasal Wash and Serum Samples

The types of antibody present in the nasal wash and serum samples were examined after fractionation on a gel filtration column. The concentrated nasal wash samples (100 μl, about 6 mg/ml) and diluted serum samples (10-fold diluted sera, 100 μl, about 6 mg/ml) were fractionated on a Superose 6 column in PBS. The antibody concentration in each fraction was then measured by ELISA. Figure 2 shows the profiles for IgM, IgA, and IgG antibodies, together with the absorbance values for the total protein in each fraction. The nasal wash samples contained IgM, which comprised less than 1% of the total protein and showed a peak MW of 970 kD; IgA, which comprised about 20% of the total protein and showed a peak MW of about 660 kD; and IgG, which comprised about 6% of the total protein and showed a peak MW of 150 kD. The MW of the nasal IgA (150 kD–900 kD, with a peak MW of 660 kD) appeared to correspond to that of tetrameric IgA (the MW of dimeric IgA is estimated to be about 360 kD). The maximum absorbance value observed in the protein profile (at around 66 kD) was due to the presence of human serum albumin (Fig. 2A).

The serum samples contained IgM, which comprised about 3% of the total protein and showed a peak MW of 970 kD; IgA, which comprised about 6% of the total protein and showed a peak MW of about 150 kD; and IgG, which comprised about 23% of the total protein and showed a peak MW of 150 kD

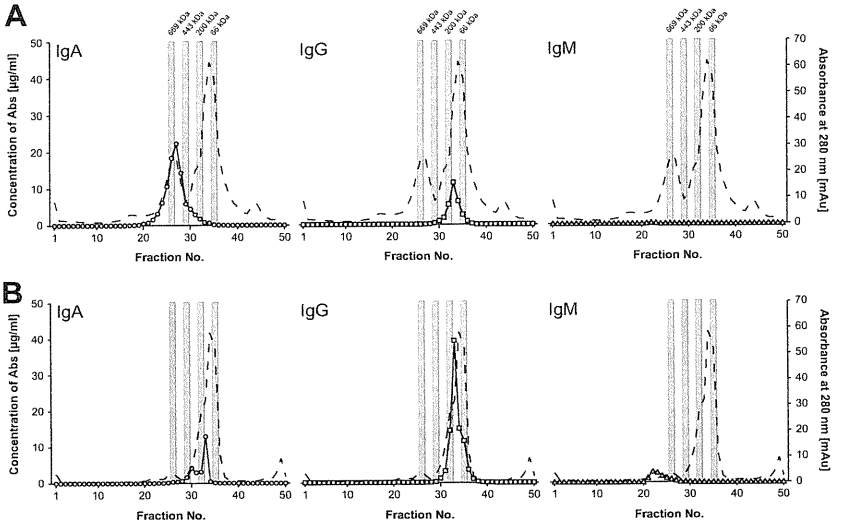


Fig. 2. Fractionation of nasal wash (**A**) and serum (**B**) samples from representative participants on Superose 6 columns. Quantification (μg/ml) of IgA (open circles), IgG (open squares), or IgM (open triangles) antibody levels and the absorbance at 280 nm (mAu, broken line) are shown. The grey zones in the upper part of the curves indicate the positions of the molecular weight markers [thyroglobulin (669 kD), apoferritin (443 kD), β-amylase (200 kD), and bovine serum albumin (66 kD)].

(Fig. 2B). Serum IgA (which showed a lower peak at about 360 kD in addition to a peak at about 150 kD) appeared to comprise both monomeric and dimeric IgA.

Taken together, the results of the fractionation analysis suggests that highly polymeric IgA is the predominant nasal antibody, and can be separated from nasal IgG and IgM. By contrast, the monomeric forms of IgG are the major component of total serum antibodies.

### Neutralization Activity of the IgA and IgG Antibodies in The Nasal Wash and Serum Samples

To determine the isotype of the antibodies responsible for the neutralization activity induced by intranasal administration of the inactivated vaccine, nasal wash and serum samples from participant P1, who showed relatively high neutralization titres after the fifth vaccination, were separated on a Superose 6 column and the neutralization titre of the resulting antibody fractions assayed. The nasal polymeric IgA fraction (No. 27) showed a neutralization titre of 1:10, whereas the nasal monomeric IgG fraction (No. 33) showed a reciprocal neutralization titre of <1:10. However, the serum dimeric IgA fraction (No. 30) showed a neutralization titre of <1:10, whereas the serum peak monomeric IgG fraction (No. 33) showed a neutralization titre of 1:10 (Table IV). The respective peak fractions in the nasal wash were then concentrated to 100 μg/ml, and the neutralization activity of the nasal IgA antibodies (a mixture of fractions 26 and 27) was compared with that of the nasal IgG antibodies (a mixture of fractions 33 and 34). The nasal IgA fractions showed a neutralization titre of 1:40, whereas the nasal monomeric IgG fractions showed a neutralization titre of 1:10. Similarly, the neutralization activity of the serum IgA antibodies (100 μg/ml; a mixture of fractions 30 and 31) was compared with that of serum IgG antibodies (a mixture of fractions 33 and 34). The serum IgA fractions showed a neutralization titre of <1:10, whereas the serum

TABLE IV. Neutralization Titre of the IgA and IgG Fractions From the Nasal Wash and Serum Samples Following Separation on Superose Columns

| | Neutralization titre[a] | | | |
|---|---|---|---|---|
| | Nasal wash | | Serum | |
| | Polymeric IgA | IgG | Dimeric IgA | IgG |
| A/Uruguay (A/H3N2) | | | | |
| Peak fraction: Separated on Superose column | 10 (0) | <10 (<0) | <10 (<0) | 10 (0) |
| Concentrated fraction (100 μg/ml) | 40 (2) | 10 (0) | <10 (<0) | 10 (0) |

The samples were collected from a representative subject vaccinated five times with an interval of 3 weeks between vaccinations.
[a]Respective values are a reciprocal titre and a geometric titre ($10 \times 2^n$) in a parenthesis.

IgG fractions showed a neutralization titre of 1:10 (Table IV).

The peak polymeric IgA fraction (about 600 kD) from the nasal wash samples, as measured using an IgA ELISA, contained no IgG antibodies when measured using an IgG ELISA; however, the peak monomeric IgG fractions (about 150 kD) from the nasal wash comprised about 1/4 of IgA (data not shown). By contrast, about 1/10 of the peak dimeric IgA (about 380 kD) from the serum samples comprised IgG antibodies, whereas about 1/10 of the peak monomeric IgG fractions from the serum comprised IgA (data not shown). This suggests that nasal polymeric IgA is responsible for the neutralization activity observed in the peak polymeric IgA fractions (about 600 kD) from the nasal wash samples. Serum monomeric IgG appears to be responsible for the neutralization activity observed in the peak monomeric IgG fractions (about 150 kD) from the serum, because the IgA content of the IgG fractions was very small. In those nasal monomeric IgG fractions that contained a relatively high amount of IgA, both IgG and IgA may be responsible for the neutralization activity. Taken together, these results show that the main neutralizing antibody in the nasal mucus is highly polymeric IgA, while the main neutralizing antibody in the serum is monomeric IgG.

## DISCUSSION

In the present study, neutralizing antibody responses and their properties were examined in nasal and serum samples from healthy adults after intranasal administration of a concentrated, inactivated split A/Uruguay (H3N2) vaccine (containing 45 μg HA per dose). The first intranasal administration of a concentrated split vaccine in young adults was conducted by Kuno-Sakai et al. [1994] and showed that both serum HI- and nasal HA-specific IgA antibodies were induced after two aerosol vaccinations, which protected against a challenge infection with a cold-adapted live virus vaccine. In the present trial, neutralizing antibody responses were examined in both serum and nasal wash samples obtained from adults given five doses of vaccine, with an interval of 3 weeks between doses. The nasal wash samples were concentrated to ensure that nasal and serum neutralization titres were assayed at equivalent levels (Table I).

To measure the concentration of IgA and IgG antibodies in the concentrated nasal wash samples, the standardized nasal wash samples were adjusted to 1 mg/ml of total protein, and contained about 1/10 amount of IgA and IgG found in natural nasal mucus [Kurono and Mogi, 1987]. Previous studies show that the total amounts of IgA and IgG increase between pre-vaccination and post-vaccination in BALB/c mice [Tamura et al., 1990, 2010]; however, the results of the present study show that the amount of total IgA (and other antibodies) recovered from the nasal mucus showed small variations at each sampling time, although this was not related to vaccination status (data not shown). Even allowing for small variations in the recovery of total IgA and IgG from the nasal mucus of each subject, the neutralization titres in the standardized nasal wash samples after vaccination appeared to be a reasonable reflection of the absolute antibody titre in the nasal mucus.

A $\geq$4-fold increase in the nasal neutralization titre was observed after the second vaccination in the four younger subjects, whereas a rise in the serum neutralization titre was observed only after the fifth vaccination in the three younger subjects (Table II and Fig. 1). Intranasal administration of a vaccine tends to induce inferior serum antibody responses, but superior nasal IgA responses, compared with intramuscular injection [Atmar et al., 2007]. The present study also showed that neutralization titres correlated well with HI titres, although the HI titres were lower than the corresponding neutralization titres (Table III). This result confirms the work of Okuno et al. [1990], who showed that HI titres are sometimes lower than the corresponding neutralization titres, depending on the strain of influenza A or B virus used in the HI assay.

Healthy adults who had already acquired immunity to influenza viruses due to previous natural infections or vaccinations (seropositive adults) showed both nasal and serum antibody responses induced by the nasal vaccine (Tables II and III, and Fig. 1). Clinical trials show that intranasal administration of inactivated vaccines induces both mucosal and systemic antibody responses in seropositive adults [Kuno-Sakai et al., 1994; Hashigucci et al., 1996; Muszkat et al., 2000; Greenbaum et al., 2002; Durrer et al., 2003; Treanor et al., 2006; Atmar et al., 2007]. The induction of antibody responses in seropositive people by the nasal vaccine can be explained by the notion that the seropositive people have immunological memory for influenza viruses. Previous reports show that administration of an intranasal split vaccine plus adjuvant induces both local and systemic antibody responses in naive mice, and that the adjuvant is not required for a booster dose to induce an enhanced anamnestic immune response 4 weeks later [Tamura et al., 1989, 1992]. Administration of an adjuvant together with the vaccine stimulates innate immunity via several classes of pattern-recognition receptors (such as Toll-like receptors), which leads to the acquisition of specific immune responses, including immunological memory [Tamura et al., 1991, 2005; Tamura and Kurata, 2004].

Analysis of nasal wash and serum samples after passage through Superose 6 columns showed that the major component of nasal mucus antibodies was highly polymeric IgA, while that of serum antibodies was IgG (Fig. 2). In those subjects that received five doses of the intranasal A/Uruguay (H3N2) vaccine, the highly polymeric nasal IgA fractions were responsible for the majority of the neutralizing activity, whereas

the serum IgG fractions were responsible for the majority of the neutralizing activity in the serum (Table IV). These data are in agreement with those obtained in a previous mouse model experiment, in which IgA antibodies with neutralizing activity purified from the respiratory tract of mice immunized intranasally with HA molecules from the A/Puerto Rico/8/34 (H1N1) virus were polymeric, whereas the purified IgG antibodies with neutralizing activity were monomeric [Tamura et al., 1990]. Further study of the detailed structure of IgA, which has higher MW than expected for dimeric IgA [Song et al., 1995] remains to be performed.

Previous studies show that IgA in the respiratory tract is more cross-reactive with variant influenza viruses than IgG [Tamura et al., 1990, 1991]. This cross-reactivity seems to depend on the polymeric nature of IgA [Taylor and Dimmock, 1985; Palladino et al., 1995]. Taken together, these data suggest the potential for intranasally administered inactivated vaccines to induce cross-protection against antigenic variants of viruses in pre-immunized adults.

Both serum and mucosal HA-specific ELISA antibody responses after nasal vaccination need to be examined and compared with the corresponding neutralization and HI titres. In addition, neutralizing antibody responses to other influenza vaccines (from different strains, different subtypes or types of viruses, and from different forms of vaccines such as subvirion and whole virus vaccines) after nasal vaccination remain to be examined to compare the efficacy of nasal vaccines with that of the parenteral vaccine. Some of these studies are ongoing.

In conclusion, intranasal administration of an A/Uruguay split vaccine containing 45 μg HA resulted in induced nasal and serum neutralizing antibody responses in four out of five healthy adult subjects, with a neutralization titre of >1:40 after the second and the fifth administrations, respectively. These neutralizing antibody responses were largely due to the induction of nasal polymeric IgA and serum monomeric IgG.

## ACKNOWLEDGMENTS

We express our appreciation to all the study participants and thank the authors whose work is cited in this paper. We would also like to thank Mr Patrick Costigan for proofreading.

## REFERENCES

Asahi Y, Yoshikawa T, Watanabe I, Iwasaki T, Hasegawa H, Sato Y, Shimada S, Nanno M, Matsuoka Y, Ohwaki M, Iwakura Y, Suzuki Y, Aizawa C, Sata T, Kurata T, Tamura S. 2002. Protection against influenza virus infection in polymeric Ig receptor knockout mice immunized intranasally with adjuvant-combined vaccines. J Immunol 168:2930–2938.

Asahi-Ozaki Y, Yoshikawa T, Iwakura Y, Suzuki Y, Tamura S, Kurata T, Sata T. 2004. Secretory IgA antibodies provide cross-protection against infection with different strains of influenza B virus. J Med Virol 74:328–335.

Atmar RL, Keitel WA, Cate TR, Munoz FM, Ruben F, Couch RB. 2007. A dose-response evaluation of inactivated influenza vaccine given intranasally and intramuscularly to healthy young adults. Vaccine 25:5367–5373.

Belshe RB, Gruber WC, Mendelman PM, Mehta HB, Mahmood K, Reisinger K, Treanor J, Zangwill K, Hayden FG, Bernstein DI, Kotloff K, King J, Piedra PA, Block SL, Yan L, Wolff M. 2000. Correlates of immune protection induced by live, attenuated, cold-adapted, trivalent, intranasal influenza virus vaccine. J Infect Dis 181:1133–1137.

Brandtzag P, Krajci P, Lamm ME, Kaetzl CS. 1994. Epitherial and hepatobiliary transort of polymeric immunogloburins. In: Ogra PL, Mestecky J, Lamm ME, Strober W, McGee JR, Bienenstock J, editors. Handbook of mucosal immunology. San Diego: Academic Press, pp 113–126.

Davenport FM, Hennessy AV, Brandon FM, Webster RG, Barrett CD Jr, Lease GO. 1964. Comparisons of serologic and febrile responses in humans to vaccination with influenza a viruses or their hemagglutinins. J Lab Clin Med 63:5–13.

Durrer P, Gluck U, Spyr C, Lang AB, Zurbriggen R, Herzog C, Gluck R. 2003. Mucosal antibody response induced with a nasal virosome-based influenza vaccine. Vaccine 21:4328–4334.

Greenbaum E, Furst A, Kiderman A, Stewart B, Levy R, Schlesinger M, Morag A, Zakay-Rones Z. 2002. Mucosal [SIgA] and serum [IgG] immunologic responses in the community after a single intra-nasal immunization with a new inactivated trivalent influenza vaccine. Vaccine 20:1232–1239.

Hashigucci K, Ogawa H, Ishidate T, Yamashita R, Kamiya H, Watanabe K, Hattori N, Sato T, Suzuki Y, Nagamine T, Aizawa C, Tamura S, Kurata T, Oya A. 1996. Antibody responses in volunteers induced by nasal influenza vaccine combined with Escherichia coli heat-labile enterotoxin B subunit containing a trace amount of the holotoxin. Vaccine 14:113–119.

Hierholzer JC, Suggs MT, Hall EC. 1969. Standardized viral hemagglutination and hemagglutination-inhibition tests. II. Description and statistical evaluation. Appl Microbiol 18:824–833.

Ito R, Ozaki YA, Yoshikawa T, Hasegawa H, Sato Y, Suzuki Y, Inoue R, Morishima T, Kondo N, Sata T, Kurata T, Tamura S. 2003. Roles of anti-hemagglutinin IgA and IgG antibodies in different sites of the respiratory tract of vaccinated mice in preventing lethal influenza pneumonia. Vaccine 21:2362–2371.

Kadowaki S, Chen Z, Asanuma H, Aizawa C, Kurata T, Tamura S. 2000. Protection against influenza virus infection in mice immunized by administration of hemagglutinin-expressing DNAs with electroporation. Vaccine 18:2779–2788.

Kuno-Sakai H, Kimura M, Ohta K, Shimojima R, Oh Y, Fukumi H. 1994. Developments in mucosal influenza virus vaccines. Vaccine 12:1303–1310.

Kurono Y, Mogi G. 1987. Secretory IgA and serum type IgA in nasal secretion and antibody activity against the M protein. Ann Otol Rhinol Laryngol 96:419–424.

Lu BL, Webster RG, Hinshaw VS. 1982. Failure to detect hemagglutination-inhibiting antibodies with intact avian influenza virions. Infect Immun 38:530–535.

Murphy BR. 1994. Mucosal Immunity to Viruses. In: Ogra PL, Mestecky J, Lamm ME, Strober W, McGee JR, Bienenstock J, editors. Handbook of mucosal immunology. San Diego: Academic Press. pp 333–343.

Murphy BR, Clements ML. 1989. The systemic and mucosal immune response of humans to influenza A virus. Curr Top Microbiol Immunol 146:107–116.

Murphy BR, Webster RG. 1996. Orthomyxoviruses. In: Fields BN, Knipe DM, M HP, Chanock RM, Melnick JL, Monath TP, Roizman B, Straus SE, editors Fields virology. 3rd edition. Philadelphia: Lippincott Williams & Wilkins. pp 1397–1445.

Muszkat M, Yehuda AB, Schein MH, Friedlander Y, Naveh P, Greenbaum E, Schlesinger M, Levy R, Zakay-Rones Z, Friedman G. 2000. Local and systemic immune response in community-dwelling elderly after intranasal or intramuscular immunization with inactivated influenza vaccine. J Med Virol 61:100–106.

Okuno Y, Tanaka K, Baba K, Maeda A, Kunita N, Ueda S. 1990. Rapid focus reduction neutralization test of influenza A and B viruses in microtiter system. J Clin Microbiol 28:1308–1313.

Palladino G, Mozdzanowska K, Washko G, Gerhard W. 1995. Virus-neutralizing antibodies of immunoglobulin G (IgG) but not of IgM or IgA isotypes can cure influenza virus pneumonia in SCID mice. J Virol 69:2075–2081.

Ramphal R, Cogliano RC, Shands JW Jr, Small PA Jr. 1979. Serum antibody prevents lethal murine influenza pneumonitis but not tracheitis. Infect Immun 25:992–997.

Renegar KB, Jackson GD, Mestecky J. 1998. In vitro comparison of the biologic activities of monoclonal monomeric IgA, polymeric IgA, and secretory IgA. J Immunol 160:1219–1223.

Renegar KB, Small PA Jr, Boykins LG, Wright PF. 2004. Role of IgA versus IgG in the control of influenza viral infection in the murine respiratory tract. J Immunol 173:1978–1986.

Rowe T, Abernathy RA, Hu-Primmer J, Thompson WW, Lu X, Lim W, Fukuda K, Cox NJ, Katz JM. 1999. Detection of antibody to avian influenza A (H5N1) virus in human serum by using a combination of serologic assays. J Clin Microbiol 37:937–943.

Song W, Vaerman JP, Mostov KE. 1995. Dimeric and tetrameric IgA are transcytosed equally by the polymeric Ig receptor. J Immunol 155:715–721.

Tamura S, Funato H, Hirabayashi Y, Kikuta K, Suzuki Y, Nagamine T, Aizawa C, Nakagawa M, Kurata T. 1990. Functional role of respiratory tract haemagglutinin-specific IgA antibodies in protection against influenza. Vaccine 8:479–485.

Tamura S, Funato H, Hirabayashi Y, Suzuki Y, Nagamine T, Aizawa C, Kurata T. 1991. Cross-protection against influenza A virus infection by passively transferred respiratory tract IgA antibodies to different hemagglutinin molecules. Eur J Immunol 21:1337–1344.

Tamura S, Hasegawa H, Kurata T. 2010. Estimation of the effective doses of nasal-inactivated influenza vaccine in humans from mouse-model experiments. Jpn J Infect Dis 63:8–15.

Tamura S, Kurata H, Funato H, Nagamine T, Aizawa C, Kurata T. 1989. Protection against influenza virus infection by a two-dose regimen of nasal vaccination using vaccines combined with cholera toxin B subunit. Vaccine 7:314–320.

Tamura S, Kurata T. 2004. Defense mechanisms against influenza virus infection in the respiratory tract mucosa. Jpn J Infect Dis 57:236–247.

Tamura S, Tanimoto T, Kurata T. 2005. Mechanisms of broad cross-protection provided by influenza virus infection and their application to vaccines. Jpn J Infect Dis 58:195–207.

Tamura SI, Asanuma H, Ito Y, Hirabayashi Y, Suzuki Y, Nagamine T, Aizawa C, Kurata T, Oya A. 1992. Superior cross-protective effect of nasal vaccination to subcutaneous inoculation with influenza hemagglutinin vaccine. Eur J Immunol 22:477–481.

Taylor HP, Dimmock NJ. 1985. Mechanism of neutralization of influenza virus by secretory IgA is different from that of monomeric IgA or IgG. J Exp Med 161:198–209.

Tobita K, Sugiura A, Enomote C, Furuyama M. 1975. Plaque assay and primary isolation of influenza A viruses in an established line of canine kidney cells (MDCK) in the presence of trypsin. Med Microbiol Immunol 162:9–14.

Treanor J, Nolan C, O'Brien D, Burt D, Lowell G, Linden J, Fries L. 2006. Intranasal administration of a proteosome-influenza vaccine is well-tolerated and induces serum and nasal secretion influenza antibodies in healthy human subjects. Vaccine 24:254–262.

Biochemical and Biophysical Research Communications 414 (2011) 719–726

Contents lists available at SciVerse ScienceDirect

Biochemical and Biophysical Research Communications

journal homepage: www.elsevier.com/locate/ybbrc

# A novel function of the N-terminal domain of PA in assembly of influenza A virus RNA polymerase

Tadaki Suzuki [a], Akira Ainai [b], Noriyo Nagata [a], Tetsutaro Sata [a], Hirofumi Sawa [c], Hideki Hasegawa [a,*]

[a] Department of Pathology, National Institute of Infectious Diseases, Musashimurayama 208-0011, Japan
[b] Influenza Virus Research Center, National Institute of Infectious Diseases, Musashimurayama 208-0011, Japan
[c] Department of Molecular Pathobiology, Hokkaido University Research Center for Zoonosis Control, Global COE Program, Sapporo 001-0020, Japan

ARTICLE INFO

*Article history:*
Received 21 September 2011
Available online 6 October 2011

*Keywords:*
Influenza A virus
Viral RNA polymerase
Polymerase complex assembly

ABSTRACT

Transcription and replication of the negative-sense single-stranded influenza A virus genomic viral RNA are catalyzed by the viral RNA polymerase, which is a trimeric complex encoded by the three largest segments of the influenza virus genome: PB1, PB2, and PA. Numerous studies of the trimeric polymerase complex assembly have substantially contributed to current understanding of influenza virus replication. However, the dynamics of spatial and temporal macromolecular interactions involving virus and host proteins during the formation of the trimeric polymerase complex (PA–PB1–PB2) are still not completely understood.

In this study, bimolecular fluorescence complementation (BiFC) and Raster image correlation spectroscopy (RICS) were applied to monitor the interactions between PB1, PB2, and PA. The BiFC probes of PA–PB1 and PB1–PB2 could monitor the trimeric polymerase complex as well as the binary complex. Furthermore, the C-terminal domain of PA (PAC) promoted interaction between PB1 and PB2 in the cytoplasm and that the N-terminal domain of PA (PAN) inhibited the aberrant trimeric complex formation and assembly of higher-order oligomers induced by PAC in the cytoplasm. Taken together, these results revealed a novel function of PAN in the formation of the trimeric polymerase complexes of influenza A virus.

© 2011 Elsevier Inc. All rights reserved.

## 1. Introduction

The influenza A virus genome is transcribed and replicated by the trimeric viral RNA polymerase (PA, PB1, and PB2) in the nuclei of infected cells. Therefore, the polymerase subunits have to be imported into the nuclei and assembled into a functional trimer [1].

Recently, a novel bio-imaging technique, fluorescence cross-correlation spectroscopy (FCCS), was applied to monitor the interactions between the polymerase subunits as well as their spatial and temporal relationships in live cells [2]. This technique confirmed the model of assembly and nuclear import of the influenza A polymerase complex proposed by Deng et al. [3], in that a PA–PB1 heterodimer is imported into the nucleus, where it then associates with the independently imported PB2 to form the fully assembled trimeric polymerase in the nucleus. Furthermore, the FCCS clearly showed that trimeric complexes could form higher-order oligomers. However, the FCCS using each of polymerase subunits labeled individually with fluorescent protein could not detect the detailed subcellular localization of the complexes formed, since the signal from dimers/trimers was indistinguishable from that of monomers.

The bimolecular fluorescence complementation (BiFC) assay enables direct visualization of protein interactions in live cells [4]. Recently, Hemerka et al. developed and validated a BiFC approach to detect the formation of pairwise binary complexes of polymerase (PA–PB1, PB1–PB2 or PA–PB2) [5]. However, the behavior of these binary complexes under the condition of triple co-expression of polymerase subunits (PA, PB1, and PB2) has not been demonstrated.

In this study, we applied BiFC and Raster image correlation spectroscopy (RICS), which is a technique for measuring molecular dynamics and concentrations from fluorescence confocal images [6], to monitor the interactions between the subunits of influenza A virus RNA polymerase in live cells. The BiFC probes, which detected PA–PB1 or PB1–PB2 interaction, demonstrated that triple co-expression of PB1, PB2, and PA influenced the localization and mobility of polymerase complexes in agreement with previous reports [3,5,7]. Furthermore, BiFC experiments using deletion mutants indicated that the N-terminal domain of PA (PAN) inhibited both PB1–PB2 interaction and formation of higher-order oligomers induced by the C-terminal domain of PA (PAC) in the cytoplasm.

*Abbreviations:* BIFC, bimolecular fluorescence complementation; RICS, Raster image correlation spectroscopy; FCCS, fluorescence cross-correlation spectroscopy.

* Corresponding author. Fax: +81 42 561 6572.
*E-mail address:* hasegawa@nih.go.jp (H. Hasegawa).

0006-291X/$ - see front matter © 2011 Elsevier Inc. All rights reserved.
doi:10.1016/j.bbrc.2011.09.142

## 2. Materials and methods

### 2.1. Construction of plasmids

PA, PB1 and PB2 expression plasmids derived from influenza H1N1 A/PuertoRico/8/34 (PR8) virus reverse genetics systems were kindly provided by Dr. Ayato Takada at Hokkaido University. For the construction of BiFC plasmids, the complementary DNAs (cDNAs) of polymerase subunits were amplified by polymerase chain reaction using the PA, PB1, and PB2 expression plasmids as templates and sub-cloned into pCXSN plasmid [8]. Sequences encoding the amino [residues 1–173 (VN)] or the carboxyl [residues 155–228 (VC)] fragments of Venus fluorescence protein (kindly provided by Dr. A. Miyawaki) were fused to the C-terminus of each of the three subunits (PA, PB1, and PB2) or deletion mutants derived from PA (PAN: residues 1–240, PAC: residues 240–716), or PB2 (PB2N: residues 1–259) via linker sequences (NSRTKLGSAAANSADGGGGSGGSGGSGGGGSTQGTGGS). The cDNAs of PA, PB2, PAN (residues 1–240) and PAC (residues 240–716) were also sub-cloned into the pCXSN-MycC plasmid [8] for expression of the C-terminal Myc-tagged polymerase subunits. Integrity of the plasmids was verified by sequencing. CFP, cyan fluorescent protein (kindly provided by Dr. A. Miyawaki), was sub-cloned into the pCXSN-MycC plasmid.

### 2.2. Cell culture and transfection

Human embryonic kidney 293 cells with SV40 T antigen (293T) were obtained from the Health Science Research Resources Bank (HSRRB). The cells were maintained under 5% $CO_2$ at 37 °C in Dulbecco's minimal essential medium supplemented with 10% heat-inactivated fetal bovine serum, 2 mM L-glutamine, penicillin and streptomycin (Sigma). The cells, grown on 35-mm glass-bottomed dishes (for imaging) or 96-well plates (for flow cytometry), were transiently transfected using FuGENE HD (Roche, Mannheim, Germany) following the procedures outlined by the manufacturer.

### 2.3. Flow cytometry

293T cells were transfected with BiFC constructs and CFP as a transfection control. At 48 h post-transfection, cells were trypsinized and resuspended in 500 μl of phosphate-buffered saline (PBS) followed by analysis with a FACSCanto II machine (Becton Dickinson, NJ). Cells transfected with CFP plasmid alone were used to set the baseline for fluorescence detection.

### 2.4. Fluorescence microscopy

Transfected 293T cells were fixed with 3% paraformaldehyde in PBS followed by nuclei staining for 1 min with 4′6-diamidino-2-phenylindole (DAPI) (Molecular Probes, Eugene, OR). The cells were observed with a confocal laser-scanning microscope, FV1000-D (Olympus, Tokyo, Japan). For quantification of the localization pattern of BiFC signal, the cells were imaged using an inverted fluorescence microscopy (Olympus) equipped with a cooled charge coupled device camera (Olympus). The integrated fluorescence intensities in the nucleus or cytoplasm of a single cell were analyzed by the Multi Wavelength Cell Scoring Application Modules of MetaMorph software (Molecular devices, CA).

### 2.5. Raster image correlation spectroscopy (RICS)

For RICS data acquisition, the transfected cells were placed in a chamber box on a microscope, in which the temperature was maintained at 37 °C, and were imaged using the FV1000-D microscope with a 60× 1.35 NA oil objective (Olympus). The scan speed was set at 10.0 μs/pixel. The scan area was 256 × 256 pixels and approximately 100 frames were collected for each sample. The electronic zoom of the microscope was set to 16.4, which corresponds to a region of 12.5 $\mu m^2$ (the pixel size was 50 nm). For the Venus excitation, the 515 nm line of the argon ion laser was used. Data were collected in the pseudo photon counting mode of the FV1000-D microscope. For analyzing RICS data, the RICS analysis package available for Fluoview1000 (Diffusion Measurement Package for the Olympus FluoView FV1000 Confocal Microscope) was used and analysis was performed by subtracting the moving average mode following the procedures outlined by the manufacturer. Under this condition, the diffusion coefficient of Venus fluorescence protein in the cytoplasm was 25.1 ± 7.2 $\mu m^2/s$, in agreement with previous studies using other methods [9].

### 2.6. Statistical analysis

All data were expressed as mean values ± S.D. The Student's *t*-test was used to analyze differences between two groups.

## 3. Results

### 3.1. Detection of PA–PB1 interactions in the trimeric polymerase complex

We initially studied spatial and temporal dynamics of PA–PB1 interaction upon the formation of the trimeric polymerase complex using BiFC. For the BiFC analysis, we generated chimeric constructs of PA and PB1 fused with the N-terminal region of Venus (VN; 1–173 a.a.) or the C-terminal region of Venus (VC; 155–228 a.a.). Venus, a variant of enhanced yellow fluorescent protein, was previously demonstrated to have strong fluorescence in BiFC analysis [5]. Previous reports indicated that fusion of GFP to the C-terminus of either the PA or PB1 proteins does not interfere with native protein function [10,11]; therefore, we generated BiFC constructs of PA and PB1 by fusing the VN and VC fragments to the C-terminus of both proteins. The resulting fusion constructs were designated PA-VN, PA-VC, PB1-VN, and PB1-VC, respectively (Fig. 1A).

293T cells were co-transfected with several combinations of the BiFC constructs and a CFP plasmid, which was used as a control to account for the efficiency of transfection and other experimental variables. Flow cytometry was used to determine the number of Venus-expressing cells (fluorescence complementation due to PA–PB1 interaction) relative to the number of CFP-expressing cells. The cells expressing CFP alone or without transfection (NT) had no detectable Venus fluorescence (Fig. 1B). However, obvious Venus fluorescence was observed when the cells were transfected with a combination of PA-VC and PB1-VN, indicating Venus fragment complementation triggered by PA–PB1 interaction (Fig. 1C and D). Furthermore, the combination of PA-VN with PB1-VC also showed positive signals for Venus (Fig. 1C and D), suggesting of exchangeability of the Venus fragments.

To determine whether PB2 co-expression influenced the formation of the PA–PB1 dimeric complex, we performed flow cytometry with cells transfected with Myc-tagged PB2. The BiFC signal with PB2 was similar to that without PB2 (Fig. 1C and D), suggesting that PB2 does not have a marked effect on the interaction between PA and PB1.

Confocal microscopy analysis of the subcellular localization of the PA–PB1 complex was performed with 293T cells transfected with a combination of constructs, PA-VC/PB1-VN or PA-VN/PB1-VC. The BiFC signal representing the PA–PB1 complexes was more intense in the nuclei than in the cytoplasm of the cells without PB2, while it was exclusively detected in the nuclei when in the

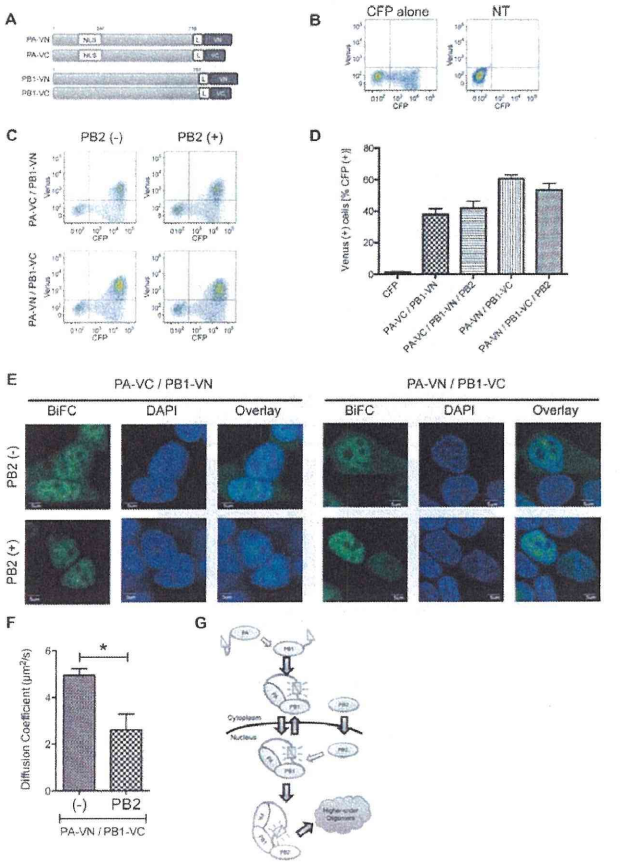


**Fig. 1.** Visualization of the PB1–PA interaction by BiFC. (A) Schematic representation of BiFC fusion proteins used in the experiment. "L" indicates a flexible linker sequence. "NLS" indicates a nuclear localization signal. (B and C) Quantitative analysis by flow cytometry with BiFC probes, PA-VC/PB1-VN or PA-VN/PB1-VC, in the presence or absence of PB2. NT: not transfected. (D) The graph indicates the percentage of cells expressing complemented Venus among the population of cells expressing CFP. (E) Subcellular localization of BiFC probes, PA-VC/PB1-VN or PA-VN/PB1-VC, with or without PB2. Scale bar: 5 μm. (F) Diffusion coefficient of BiFC probe set, PA-VN/PB1-VC in the presence or absence of PB2. At 48 h post-transfection, the cells were imaged with a confocal microscope to calculate the diffusion coefficient values of BiFC signal in the nuclei using the RICS approach ($^*p < 0.005$). (G) Schematic description of the interactions observed by the BiFC probe of PB1–PA.

presence of PB2 (Fig. 1E). The results were in accordance with previous reports that the nuclear accumulation of PB1 and PA is more efficient when both subunits are co-expressed in the presence of PB2 [2].

Recently, it has been proposed that the trimeric influenza virus polymerase forms higher-order oligomers with host factors in the nuclei [2]. The formation of higher-order oligomers dramatically reduces mobility as compared to freely diffusing molecules of comparable size [2]. To determine whether the PA–PB1 complex interacts with PB2 and subsequently forms higher-order oligomers, we estimated the diffusion coefficient of the complemented Venus fluorescence, representing the PA–PB1 complex, using RICS. The diffusion coefficient of the PA–PB1 complex in the nuclei of the cells co-expressed with Myc-tagged PB2 was approximately half ($2.6 \pm 0.7$ μm$^2$/s with PB2) of that in the nuclei of the cells without PB2 ($4.9 \pm 0.3$ μm$^2$/s without PB2) (Fig. 1F), indicating that the PA–PB1 complex with PB2 diffused more slowly and formed a complex approximately eight-times larger than in the absence of PB2, based on the Stokes–Einstein hydrodynamic theory [12]. This result suggested that the PA–PB1 complex bound to PB2 formed the trimeric polymerase complex, accumulated in the nuclei and assembled into higher-order oligomers (Fig. 1G).

### 3.2. Detection of PB1–PB2 interactions in the trimeric polymerase complex

We next studied the spatial and temporal dynamics of the PB1–PB2 interaction upon formation of the trimeric polymerase complex. 293T cells were co-transfected with BiFC constructs (Fig. 2A) with or without expression of Myc-tagged PA, and subsequently were subjected to flow cytometry. Cells expressing PB1-VN/PB2-VC or PB1-VC/PB2-VN showed very faint fluorescence of complemented Venus in the absence of PA (Fig. 2B, upper left column and 2C), which was not sufficient for detection by confocal microscopy (data not shown). By contrast, the Venus fluorescence was significantly higher in the cells expressing PB1-VN/PB2-VC or PB1-VC/PB2-VN in the presence of PA than that without PA (Fig. 2B, upper left column and 2C). The subcellular localization of the PB1–PB2 complex was exclusively nuclear in the presence of PA (PB1-VN/PB2-VC and PB1-VC/PB2-VN columns in Fig. 2D). These results were consistent with the previously proposed model in which PA–PB1 heterodimers formed in the cytoplasm were imported into the nuclei as a heterodimer, independently of PB2. Thereafter, the heterodimer bound to PB2 and assembled as a functional trimeric complex [3,2]. Taken together with the results shown in Fig. 1, this suggested that expression of PA was necessary for PB1–PB2 BiFC probe complementation and that the BiFC signal of the PB1–PB2 complex might represent the trimeric polymerase complex but not the PB1–PB2 dimer (Fig. 2F).

### 3.3. The C-terminal domain of PB2 is responsible for nuclear accumulation of the trimeric polymerase complex and formation of higher-order oligomers

Previous studies have proposed that a strong interaction forms between the N-terminal extremity of PB2 and the C-terminal extremity of PB1 [13]. To investigate the role of the C-terminal domain of PB2 in formation of the PB1–PB2 complex, we generated a deletion mutant of PB2, containing the N-terminal 247 amino acid residues of PB2 (PB2N) and devoid of the C-terminal NLS region (Fig. 2A).

Flow cytometry revealed that the cells transfected with the BiFC constructs including PB2N-VN or PB2N-VC without PA had significantly lower Venus fluorescence than those with PA (Fig. 2B, lower left column and 2C), suggesting that PB2N could form the trimeric complex (PA–PB1–PB2N) as well as PB2. By contrast, the subcellular localization of the PB1–PB2N complex, which was detected in the nuclei and cytoplasm with PA (PB1-VN/PB2N-VC and PB1-VC/PB2N-VN columns in Fig. 2D), was clearly different from that of PB1–PB2 complex. The results suggested that the absence of the C-terminal domain of PB2 led to aberrant formation of the trimeric complex in the cytoplasm.

To determine whether the C-terminal domain of PB2 is involved in formation of higher-order oligomers, we compared the diffusion coefficient of the PB1–PB2 complex and the PB1–PB2N complex in the presence of PA using RICS. The diffusion coefficient of the PB1–PB2N complex ($4.6 \pm 0.4$ μm$^2$/s, right bar in Fig. 2E) was significantly increased compared to that of the PB1–PB2 complex ($1.0 \pm 0.1$ μm$^2$/s, left bar in Fig. 2E), indicating that the PB1–PB2N complex was much smaller than the PB1–PB2 complex. Interestingly, the diffusion coefficient of the PB1–PB2N complex with PA ($4.6 \pm 0.4$ μm$^2$/s) was similar to that of the PA–PB1 binary complex without PB2 ($4.9 \pm 0.3$ μm$^2$/s, left bar in Fig. 1F), suggesting that the PB1–PB2N–PA complex did not assemble into intact higher-order oligomers. These results implied that the N-terminal domain of PB2 was sufficient to bind to the PB1–PA binary complex, forming the trimeric polymerase complex. The C-terminal domain of PB2 supported nuclear accumulation of the trimeric polymerase complex and assembly to higher-order oligomers (Fig. 2F).

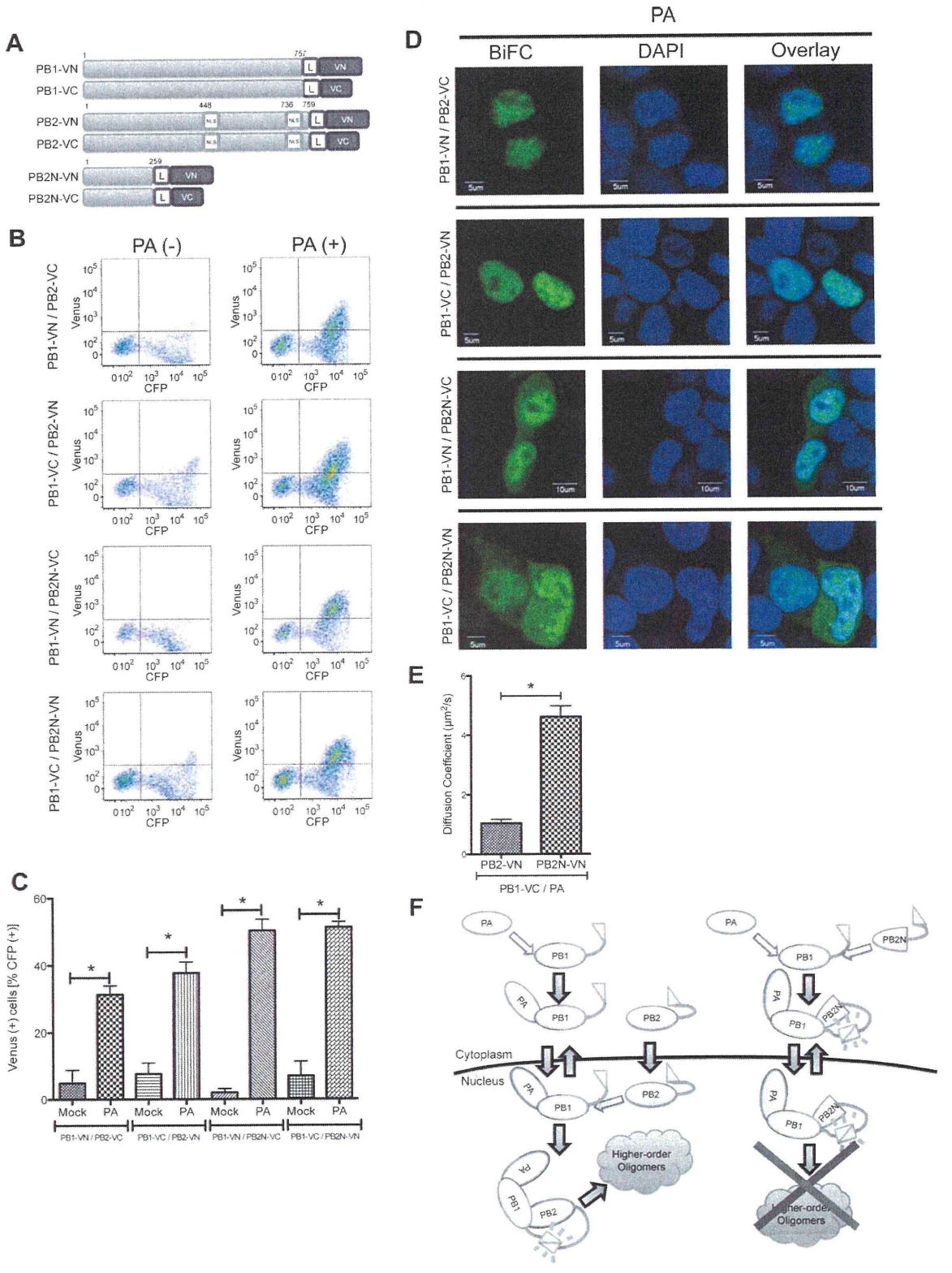


**Fig. 2.** Visualization of the PB1–PB2 and PB1–PB2N interaction by BiFC. (A) Schematic representation of BiFC fusion proteins used in this experiment. (B and C) Quantitative analysis by flow cytometry with the BiFC probes PB1-VN/PB2-VC, PB1-VC/PB2-VN, PB1-VN/PB2N-VC or PB1-VC/PB2N-VN in the presence or absence of PA (*$p < 0.001$). (D) Subcellular localization of BiFC probes, PB1-VN/PB2-VC, PB1-VC/PB2-VN, PB1-VN/PB2N-VC or PB1-VC/PB2N-VN in the presence of PA. Scale bar: 5 μm. (E) Diffusion coefficient of BiFC probes, PB1-VC/PB2-VN or PB1-VC/PB2N-VN, in the presence of PA (*$p < 0.0001$). (F) Schematic description of the interactions observed by BiFC probes of PB1–PB2 or PB1–PB2N.

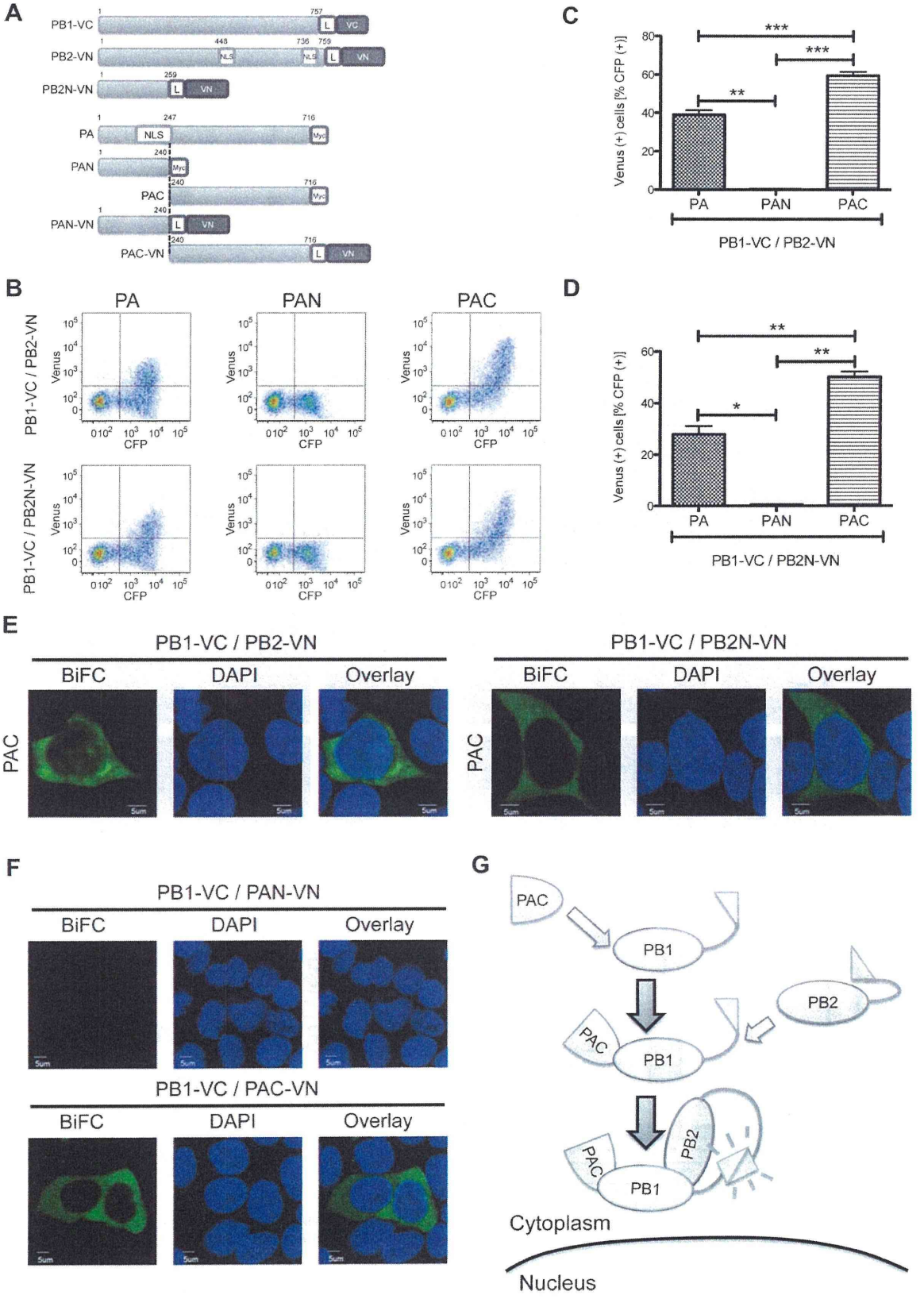


**Fig. 3.** The C-terminal domain of PA (PAC) is responsible for induction of the PB1–PB2 interaction. (A) Schematic representation of BiFC fusion proteins used in this experiment. (B–D) Quantitative analysis by flow cytometry with BiFC probes, PB1-VC/PB2-VN or PB1-VC/PB2N-VN, in the presence PA, PAN, or PAC ($^{*}p < 0.05$, $^{**}p < 0.005$, $^{***}p < 0.001$). (E) Subcellular localization of BiFC probes of PB1-VC/PB2-VN (left panel) or PB1-VC/PB2N-VN (right panel) in the presence of PAC. Scale bar: 5 μm. (F) Subcellular localization of BiFC probes, PB1-VC/PAN-VN (upper panel) or PB1-VC/PAC-VN (lower panel). Scale bar: 5 μm. (G) Schematic description of the interactions observed by BiFC probe of PB1–PB2 in the presence of PAC.

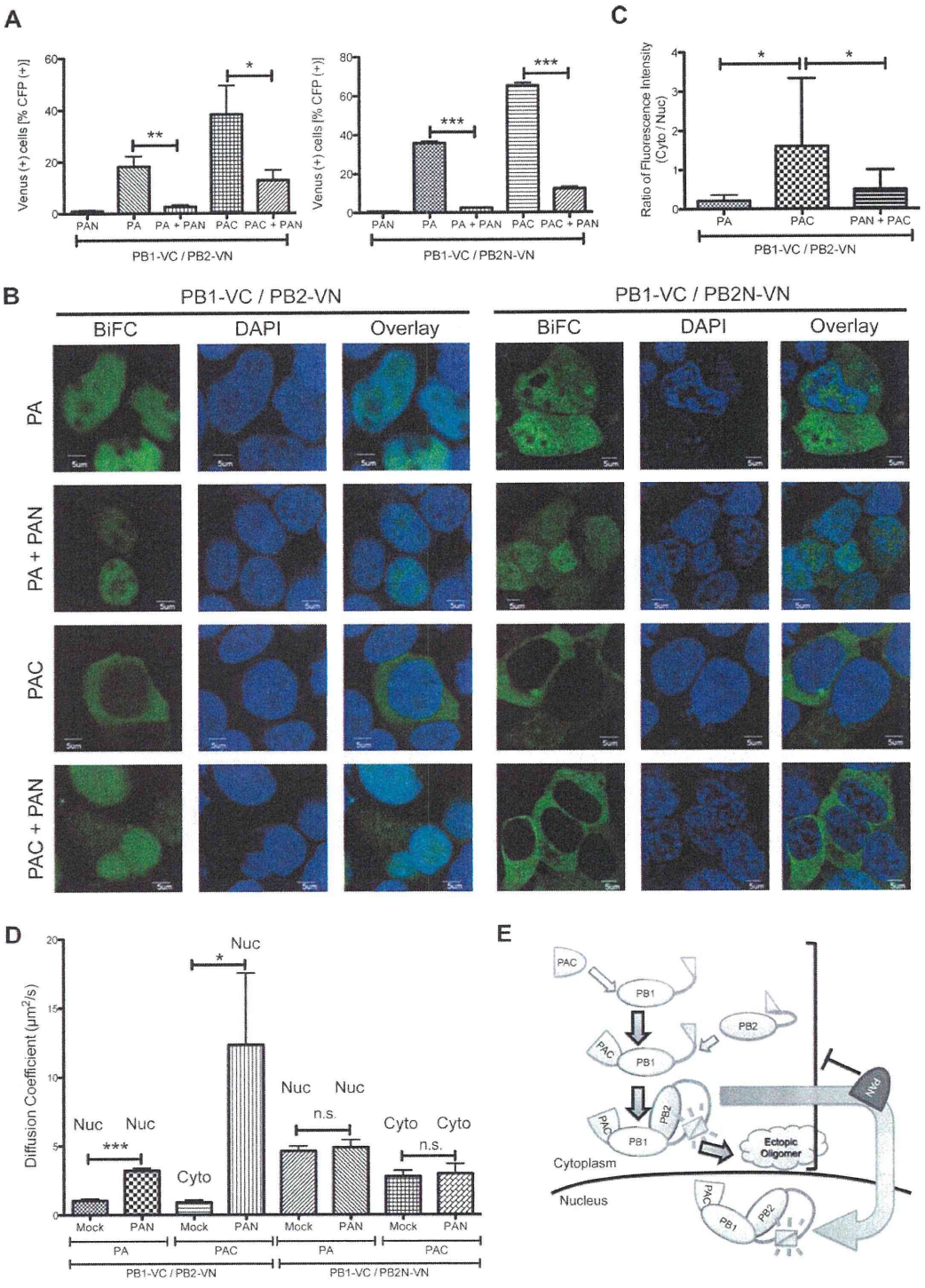


**Fig. 4.** The N-terminal domain of PA (PAN) inhibits the PB1–PB2 interaction and transfers the PAC-dependent PB1–PB2 complex to the nucleus. (A) Quantitative analysis by flow cytometry with BiFC probes, PB1-VC/PB2-VN or PB1-VC/PB2N-VN, in the combination of PAN, PA, PA + PAN, PAC or PAC + PAN. ($^{*}p < 0.05$, $^{**}p < 0.005$, $^{***}p < 0.001$). (B) Subcellular localization of BiFC probes, PB1-VC/PB2-VN (left panel) or PB1-VC/PB2N-VN (right panel), in combination with PA, PA/PAN, PAC or PAC/PAN. Scale bar: 5 μm. (C) Quantification of the subcellular localization by BiFC of the PB1–PB2 complex in the presence of PA, PAC or PAN/PAC. The bar graph indicates the ratio between the cytoplasmic and nuclear intensities of complemented Venus fluorescence. Results of cells with PA, PAC, or PAN + PAC are the mean plus standard deviation from 46, 48, or 116 cells, respectively. (D) Diffusion coefficient of BiFC probe set, PB1-VC/PB2-VN or PB1-VC/PB2N-VN, in combination with PA, PA/PAN, PAC, or PAC/PAN. "Nuc" indicates the diffusion of the target measured in the nuclei. "Cyto" indicates the diffusion of the target measured in the cytoplasm ($^{*}p < 0.05$, $^{***}p < 0.001$). (E) Schematic description of the interactions observed by BiFC probe of PB1–PB2 in the presence of PAN and PAC.

### 3.4. PAC induces aberrant PB1–PB2 interaction in the cytoplasm

The PA protein can be cleaved by limited tryptic digestion into two domains, a smaller N-terminal domain (PAN) and a larger C-terminal domain (PAC) [14]. PAC carries the PB1 binding site [15,16], whereas PAN is associated with the nuclear transport of PB1 [10].

To investigate which domain of PA induces the interaction between PB1 and PB2 in the cell, we generated plasmids encoding deletion mutants of PA, containing PAN or PAC (Fig. 3A). Flow cytometry revealed that PAC, but not PAN, induced formation of the PB1–PB2 complex (Fig. 3B and C) and the PB1–PB2N complex (Fig. 3B and D) more efficiently than PA (Fig. 3B–D). By contrast, the subcellular localization of the PB1–PB2 complex with PAC, which was mainly detected in the cytoplasm (left column in Fig. 3E), differed significantly from that with PA (PB1-VN/PB2-VC and PB1-VC/PB2-VN columns in Fig. 2E). Similarly, the PB1–PB2N complex with PAC was localized in the cytoplasm (right column in Fig. 3E). The PAC-PB1 binary complex (PB1-VC/PAC-VN column in Fig. 3F) was also localized in the cytoplasm, while the PAN–PB1 binary complex was not detected by confocal microscopy (PB1-VC/PAN-VN column in Fig. 3F). These results indicated that the binary complex consisting of PB1 and PAC was sufficient for interaction between PB1 and PB2 in the cell and that PAN played a role in the nuclear transport of PA–PB1 binary complex (Fig. 3G).

### 3.5. PAN inhibits the PB1–PB2 interaction and the formation of ectopic higher-order oligomers in the cytoplasm

To further investigate the function of PAN and PAC in the formation of the trimeric polymerase complex, we performed several assays using BiFC probes (PB1-VC/PB2-VN or PB1-VC/PB2N-VN in Fig. 3A) coupled with PA or PAC co-expression in the presence or absence of PAN. Flow cytometry revealed that PAN inhibited formation of the PB1–PB2 (left column in Fig. 4A) and PB1–PB2N complexes (right column in Fig. 4A), which were induced by PA or PAC co-expression. Confocal microscopy disclosed that the subcellular localization of the PB1–PB2 (left columns in Fig. 4B) and PB1–PB2N (right columns in Fig. 4B) complexes induced by PA was not influenced by the presence of PAN (PA + PAN in Fig. 4B). However, the subcellular localization of the PB1–PB2 complex, induced by PAC co-expression (PAC in Fig. 4B), dramatically shifted from a cytoplasmic localization pattern to a nuclear pattern in the presence of PAN (PAC + PAN in Fig. 4B and C). The shift was not observed in the PB1–PB2N complex.

To further characterize PAN function in the formation of the trimeric polymerase complex, we estimated the diffusion coefficient of the complexes under these conditions using RICS. The diffusion coefficient of the PB1–PB2 complex induced by PAC in the cytoplasm ($0.9 \pm 0.2\ \mu m^2/s$) was identical to that induced by PA in the nucleus ($1.0 \pm 0.1\ \mu m^2/s$), suggesting that the PAC–PB1–PB2 trimeric complex assembled to the higher-order oligomers in the cytoplasm. The diffusion coefficient of the PB1–PB2 complex in the presence of both PAC and PAN in the nuclei ($12.3 \pm 5.2\ \mu m^2/s$) was significantly increased compared to that of PAC alone in the cytoplasm (Fig. 4D). By contrast, the diffusion coefficient of the BiFC probes of PB1-VC and PB2N-VN, which could not form the intact higher-order oligomers in the presence of PA (Fig. 2F), was not influenced by PAN co-expression in the nucleus (Fig. 4D). These results indicated that PAN inhibited formation of the aberrant cytoplasmic higher-order oligomers induced by PAC. Taken together, these observations implied that PAN, which does not bind to PB1, might regulate the formation of the trimeric polymerase complex through inhibition of assembly of the aberrant trimeric complex in the cytoplasm (Fig. 4E).

## 4. Discussion

In this study, we applied BiFC coupled with RICS to monitor the interactions between the subunits of influenza A virus RNA polymerase in live cells and confirmed the assembly model originally proposed by Deng et al. [3]. The PA–PB1 and PB1–PB2 BiFC probes demonstrated the dynamics of not only the binary complex but also the trimeric polymerase complex *in vivo*. Furthermore, the BiFC experiments using deletion mutants indicated that PAC, which binds to PB1, induced the aberrant formation of the trimeric polymerase complex in the cytoplasm (Figs. 3E and 4B). By contrast, PAN inhibited the formation of these aberrant cytoplasmic higher-order oligomers induced by PAC and translocated the trimeric polymerase complex to the nucleus (Fig. 4B and D). PAN is the endonuclease that cleaves host mRNAs during cap-snatching [17,18]. Previous report using FCCS suggested that these higher-order oligomers consist of not only polymerase subunits but also host factors or structures [2]. It is obviously important to determine whether this inhibitory effect of PAN on the formation of oligomers depends on the endonuclease activity for elucidation the mechanism of polymerase assembly. PAN and PAC are connected by a 20-residue flexible linker [14]. The presence of the linker between the N- and C-terminal domains of PA provides a degree of conformational flexibility that may enable a role in regulating polymerase functions through conformational changes of polymerase complexes [19]. Furthermore, a weak interaction between PB2 and PAN has recently been detected using BiFC [5]. Taken together, it has been implied that PAN might interact with PB2 transiently and regulate the proper formation of the trimeric polymerase complex through inhibition of assembly of the ectopic trimeric complex in the cytoplasm. Further investigation using this BiFC approach may aid the elucidation of a novel therapeutic target for anti-influenza drugs that could inhibit polymerase assembly and activity.

## Acknowledgments

This study was supported in part by Grants from the Ministry of Education, Culture, Sports, Science and Technology; the Ministry of Health, Labor and Welfare, Japan.

## References

[1] S. Boulo, H. Akarsu, R.W. Ruigrok, F. Baudin, Nuclear traffic of influenza virus proteins and ribonucleoprotein complexes, Virus Res. 124 (2007) 12–21.
[2] S. Huet, S.V. Avilov, L. Ferbitz, N. Daigle, S. Cusack, J. Ellenberg, Nuclear import and assembly of influenza A virus RNA polymerase studied in live cells by fluorescence cross-correlation spectroscopy, J. Virol. 84 (2010) 1254–1264.
[3] T. Deng, J. Sharps, E. Fodor, G.G. Brownlee, In vitro assembly of PB2 with a PB1–PA dimer supports a new model of assembly of influenza A virus polymerase subunits into a functional trimeric complex, J. Virol. 79 (2005) 8669–8674.
[4] T.K. Kerppola, Bimolecular fluorescence complementation (BiFC) analysis as a probe of protein interactions in living cells, Annu. Rev. Biophys. 37 (2008) 465–487.
[5] J.N. Hemerka, D. Wang, Y. Weng, W. Lu, R.S. Kaushik, J. Jin, A.F. Harmon, F. Li, Detection and characterization of influenza A virus PA–PB2 interaction through a bimolecular fluorescence complementation assay, J. Virol. 83 (2009) 3944–3955.
[6] M.A. Digman, E. Gratton, Analysis of diffusion and binding in cells using the RICS approach, Microsc. Res. Tech. 72 (2009) 323–332.
[7] T. Deng, O.G. Engelhardt, B. Thomas, A.V. Akoulitchev, G.G. Brownlee, E. Fodor, Role of ran binding protein 5 in nuclear import and assembly of the influenza virus RNA polymerase complex, J. Virol. 80 (2006) 11911–11919.
[8] T. Suzuki, Y. Orba, Y. Okada, Y. Sunden, T. Kimura, S. Tanaka, K. Nagashima, W.W. Hall, H. Sawa, The human polyoma JC virus agnoprotein acts as a viroporin, PLoS Pathog. 6 (2010) e1000801.
[9] T. Matsuda, A. Miyawaki, T. Nagai, Direct measurement of protein dynamics inside cells using a rationally designed photoconvertible protein, Nat. Methods 5 (2008) 339–345.
[10] E. Fodor, M. Smith, The PA subunit is required for efficient nuclear accumulation of the PB1 subunit of the influenza A virus RNA polymerase complex, J. Virol. 78 (2004) 9144–9153.

[11] T. Naito, F. Momose, A. Kawaguchi, K. Nagata, Involvement of Hsp90 in assembly and nuclear import of influenza virus RNA polymerase subunits, J. Virol. 81 (2007) 1339–1349.
[12] D.J. Stephens, V.J. Allan, Light microscopy techniques for live cell imaging, Science 300 (2003) 82–86.
[13] K. Sugiyama, E. Obayashi, A. Kawaguchi, Y. Suzuki, J.R. Tame, K. Nagata, S.Y. Park, Structural insight into the essential PB1–PB2 subunit contact of the influenza virus RNA polymerase, EMBO J. 28 (2009) 1803–1811.
[14] T.S. Guu, L. Dong, P. Wittung-Stafshede, Y.J. Tao, Mapping the domain structure of the influenza A virus polymerase acidic protein (PA) and its interaction with the basic protein 1 (PB1) subunit, Virology 379 (2008) 135–142.
[15] E. Obayashi, H. Yoshida, F. Kawai, N. Shibayama, A. Kawaguchi, K. Nagata, J.R. Tame, S.Y. Park, The structural basis for an essential subunit interaction in influenza virus RNA polymerase, Nature 454 (2008) 1127–1131.
[16] X. He, J. Zhou, M. Bartlam, R. Zhang, J. Ma, Z. Lou, X. Li, J. Li, A. Joachimiak, Z. Zeng, R. Ge, Z. Rao, Y. Liu, Crystal structure of the polymerase PA(C)-PB1(N) complex from an avian influenza H5N1 virus, Nature 454 (2008) 1123–1126.
[17] P. Yuan, M. Bartlam, Z. Lou, S. Chen, J. Zhou, X. He, Z. Lv, R. Ge, X. Li, T. Deng, E. Fodor, Z. Rao, Y. Liu, Crystal structure of an avian influenza polymerase PA(N) reveals an endonuclease active site, Nature 458 (2009) 909–913.
[18] S. Boivin, S. Cusack, R.W. Ruigrok, D.J. Hart, Influenza A virus polymerase: structural insights into replication and host adaptation mechanisms, J. Biol. Chem. 285 (2010) 28411–28417.
[19] A. Kawaguchi, T. Naito, K. Nagata, Involvement of influenza virus PA subunit in assembly of functional RNA polymerase complexes, J. Virol. 79 (2005) 732–744.

MODERN PATHOLOGY (2012) 25, 1–13
© 2012 USCAP, Inc. All rights reserved 0893-3952/12 $32.00


# Histopathological and immunohistochemical findings of 20 autopsy cases with 2009 H1N1 virus infection

Noriko Nakajima[1], Yuko Sato[1], Harutaka Katano[1], Hideki Hasegawa[2], Toshio Kumasaka[3], Satoru Hata[4], Shinya Tanaka[5], Tomonori Amano[6], Takahiko Kasai[7], Ja-Mun Chong[8], Toshihiko Iiduka[9], Iwao Nakazato[10], Yohko Hino[11], Akihiko Hamamatsu[12], Hisashi Horiguchi[13], Tomoyuki Tanaka[14], Akio Hasagawa[15], Yoshiaki Kanaya[16], Reiko Oku[17], Takeshi Oya[18] and Tetsutaro Sata[1]

[1]*Department of Pathology, National Institute of Infectious Diseases, Tokyo, Japan;* [2]*Influenza Virus Research Center, National Institute of Infectious Diseases, Tokyo, Japan;* [3]*Department of Pathology, Japanese Red Cross Medical Center, Tokyo, Japan;* [4]*Department of Clinical Laboratory Sciences, Nagano Red Cross Hospital, Nagano, Japan;* [5]*Laboratory of Cancer Research, Department of Pathology, Hokkaido University Graduate School of Medicine, Sapporo, Japan;* [6]*Department of Cardiovascular Internal Medicine, Uji Tokushukai Hospital, Uji, Japan;* [7]*Department of Pathology, Nara Medical University Hospital, Nara, Japan;* [8]*Department of Pathology, Toshima Hospital, Tokyo, Japan;* [9]*Pathology Division of Clinical Laboratory, National Center for Global Health and Medicine, Tokyo, Japan;* [10]*Department of Pathology, Okinawa Prefectural Nanbu Medical Center and Children's Medical Center, Okinawa, Japan;* [11]*Department of Pathology, Kyoto City Hospital, Kyoto, Japan;* [12]*Tokyo Medical Examiner's Office, Tokyo, Japan;* [13]*Department of Pathology, Hitachi Ltd. Hitachinaka General Hospital, Mito, Japan;* [14]*Sakai City Institute of Public Health, Sakai, Japan;* [15]*Department of Pathology and Laboratory Medicine, Odawara Municipal Hospital, Odawara, Japan;* [16]*Department of Pediatrics, Oita Prefectural Hospital, Oita, Japan;* [17]*Department of Emergency and Intensive Care, Narita Red Cross Hospital, Narita, Japan and* [18]*Department of Pathology, Niigata Prefectural Central Hospital, Niigata, Japan*

**Twenty autopsy cases with 2009 pandemic influenza A (2009 H1N1) virus infection, performed between August 2009 and February 2010, were histopathologically analyzed. Hematoxylin–eosin staining, immunohistochemistry for type A influenza nucleoprotein antigen, and real-time reverse transcription-PCR assay for viral RNA were performed on formalin-fixed and paraffin-embedded specimens. In addition, the D222G amino acid substitution in influenza virus hemagglutinin, which binds to specific cell receptors, was analyzed in formalin-fixed and paraffin-embedded trachea and lung sections by direct sequencing of PCR-amplified products. There were several histopathological patterns in the lung according to the most remarkable findings in each case: acute diffuse alveolar damage (DAD) with a hyaline membrane (four cases), organized DAD (one case), acute massive intra-alveolar edema with variable degrees of hemorrhage (three cases), neutrophilic bronchopneumonia (five cases) and tracheobronchitis with limited histopathological changes in alveoli (four cases). In two cases, the main findings were due to preexisting disease. Influenza virus antigen was only detected in the respiratory tract in 10 cases by immunohistochemistry. The antigen was detected in type II pneumocytes (three cases) in the epithelial cells of the trachea, bronchi and glands (six cases), and in the epithelial cells in both of the above (one case). The four cases with acute DAD presented with antigen-positive type II pneumocytes. In one case, the D222G substitution was detected in the lung as a major sequence, although 222D was prominent in the trachea, suggesting that selection of the viral clones occurred in the respiratory tract. In five**

Correspondence: Dr N Nakajima, MD, PhD, Department of Pathology, National Institute of Infectious Diseases, 1-23-1 Toyama, Shinjyuku, Tokyo 162-8640, Japan.
E-mail: tenko@nih.go.jp
Received 6 April 2011; revised 24 June 2011; accepted 24 June 2011; published online 26 August 2011

**cases, the pathogenesis of 2009 H1N1 was confirmed to be viral infection in pneumocytes, which caused severe alveolar damage and fatal viral pneumonia. Further studies on both host and viral factors in autopsy or biopsy materials will be essential to elucidate the other pathogenic factors involved in influenza virus infection.**
*Modern Pathology* (2012) **25,** 1–13; doi:10.1038/modpathol.2011.125; published online 26 August 2011

**Keywords:** autopsy; histopathology; immunohistochemistry; pathogenesis; real-time RT-PCR; D222G; 2009 H1N1

Influenza virus causes respiratory infections with the potential for high morbidity and mortality, particularly in infants, the elderly, and those with underlying diseases. To control the seasonal epidemic of influenza virus infection, new vaccines are developed every year. Influenza virus also causes periodic pandemics. The emergence of avian H5N1 influenza virus infection in humans in 1997 alerted us the future outbreaks of new pandemic influenza virus infection.

In June 2009, the World Health Organization declared a novel influenza pandemic that entered the post-pandemic period in August 2010.[1] Overall, the 2009 pandemic influenza A (2009 H1N1) virus did not cause particularly severe respiratory diseases, contrary to that expected at the start of the pandemic. In most cases, it caused subclinical infections or mild-to-moderate upper respiratory tract diseases. However, in some patients, it caused severe respiratory diseases, neurological complications,[2–4] and myocardial symptoms.[5,6] The 2009 H1N1 virus caused viral pneumonia with acute respiratory distress syndrome,[7] which is not generally caused by seasonal influenza strains. It was also notable that younger people were affected with severe pneumonia, which was fatal in some cases.[8,9]

A total of 198 fatal cases with laboratory-confirmed 2009 H1N1 virus infection were reported by the Japanese Ministry of Health, Labour and Welfare, between August 2009 and March 2010. The fatality rate was estimated to be 0.001%, which was much lower than that reported in other countries.[10]

Pathological studies with autopsy materials are essential to elucidate the pathogenesis of 2009 H1N1 virus infection. Autopsy findings in fatal cases of 2009 H1N1 have been reported from several countries.[11–15] The authors of the present study also reported the pathological and virological findings of two autopsy cases of 2009 H1N1 in Japan.[16,17] Both cases revealed that the 2009 H1N1 virus infected type II pneumocytes and caused diffuse alveolar damage (DAD).

In the present study, we evaluated various histopathological features of 20 cases with 2009 H1N1 virus infection, examined the distribution of influenza nucleoprotein antigens by immunohistochemistry, and quantified viral RNA extracted from formalin-fixed and paraffin-embedded tissue specimens. For the 10 cases with viral antigen- and viral RNA-positive formalin-fixed and paraffin-embedded tissue sections, we investigated amino acid substitutions at position 222 in hemagglutinin expressed by the 2009 H1N1 virus. This position affects its receptor-binding specificity, and substitution from aspartic acid (D) to glycine (G) enables the virus to bind to the α2–3-linked sialic acid receptor (SAα2–3Gal), which is expressed in distal bronchioles and type II pneumocytes.[18–20]

## Patients and methods

### Patients

A total of 20 fatal cases with 2009 H1N1 infection were examined. Infection was confirmed by detecting viral RNA in nasopharyngeal swab specimens using the reverse-transcriptase PCR (RT-PCR) method at the first medical examination at each hospital. For six cases, the swabs were collected *post mortem* at the medical examiner's office. The autopsy tissue samples of the 20 fatal cases were sent from 15 hospitals to our laboratory for further pathological investigation between August 2009 and February 2010. Some tissue samples were formalin-fixed and others were formalin-fixed and paraffin-embedded. The tissue sections included the trachea ($n=15$), lung ($n=20$), heart ($n=10$), brain ($n=5$), liver ($n=5$), spleen ($n=5$), gastrointestinal tract ($n=5$), kidney ($n=4$), and lymph nodes ($n=3$). This study was approved by the institutional medical ethical committee of the National Institute of Infectious Diseases, Japan (Approval No. 247).

### Histopathological Studies and Immunohistochemistry Assays

Histopathological studies on formalin-fixed and paraffin-embedded specimens of all sections of 20 cases were performed using hematoxylin–eosin staining. Immunohistochemistry assays for type A influenza nucleoprotein antigen (InfA-NP) were performed to evaluate the distribution of 2009 H1N1 as described previously.[16] In brief, the sections were immunostained by the avidin–biotin complex immunoperoxidase method (LSAB2 kit/HRP/DAB, DAKO Cytomation, Copenhagen, Denmark) using a mouse monoclonal antibody against InfA-NP.[21] For double-staining with a monoclonal antibody against cell type-specific marker proteins, a rabbit polyclonal antibody against InfA-NP was used. To characterize the virus-infected cells, confocal laser scanning microscopy was used to visualize double immunofluorescence staining for

**Table 1** Clinical information of the 20 autopsy cases confirmed 2009 H1N1 virus infection

| *Case no.* | *Age/sex* | *Underlying diseases* | *Duration of illness (d)* | *Hospitalization (d)* | *Clinical symptoms* | *Antibiotic treatment* | *Antiviral treatment* | *Bacteria isolation (specimen)* |
|---|---|---|---|---|---|---|---|---|
| 1 | 33/M | Dilated cardiomyopathy, obesity (BMI: 38), diabetes, asthma, atopic dermatitis | 8 | 3 | Fever, cough, dyspnea, diarrhea | + | + | – |
| 2 | 40/F | Hypertension, obesity (BMI: 30) | 2 | NA | Fever, cough | – | – | ND |
| 3 | 45/M | Unknown | 3 | NA | Fever, general fatigue | – | – | ND |
| 4 | 49/M | Hypertension, Hashimoto's disease, obesity (BMI: 35) | 4 | NA | Fever, cough | – | – | ND |
| 5 | 30/M | CHF, alcoholic liver disease, obesity (BMI: 34) | 2 | NA | Fever, headache | – | + | ND |
| 6 | 25/M | None | 1 | NA | Fever | – | + | ND |
| 7 | 81/M | Diabetes | 3 | 2 | Fever, cough, wheezing, diarrhea, vomiting | + | + | *S. pneumoniae* (sputum) |
| 8 | 6/F | Cerebral hemorrhage, cerebral palsy, seizure | 3 | NA | Fever, dyspnea | – | + | ND |
| 9 | 42/M | Cerebral hemorrhage, hypertension, hyperlipidemia, obesity (BMI: 59), sleep apnea | 2 | NA | Fever, cough | – | – | ND |
| 10 | 75/M | Asthma, atrial fibrillation, COPD | 2 | 2 | Fever, dyspnea, wheezing | + | + | – |
| 11 | 72/F | Autoimmune hepatitis, portal hypertension, hepatic encephalopathy, pulmonary hypertension | 4 | 4 | Fever | + | + | *P. aeruginosa** (*post-mortem* lung) |
| 12 | 30/F | Asthma | 3 | 2 | Fever, diarrhea, seizures | + | + | – |
| 13 | 2/M | Hydrocephalus, laryngomalacia, mental retardation | 9 | 7 | Fever, cough | – | + | *P. aeruginosa** (*post-mortem* lung) |
| 14 | 69/M | Esophageal cancer, diabetes, COPD, CHF | 10 | 10 | Fever, cough, dyspnea | + | + | – |
| 15 | 44/M | None | 2 | 1 | Fever, VF, diarrhea, dyspnea, myalgia | – | + | – |
| 16 | 13/F | None | 3 | 1 | Cough, myalgia, headache, general fatigue | + | – | ND |
| 17 | 15/M | None | 29 (d2 PCPS) | 28 | Fever, VF | + | + | – |
| 18 | 24/F | Mental retardation | 21 (d7 ECMO) | 16 | Fever, cough, dyspnea | + | + | – |
| 19 | 33/M | Depression | 2 | NA | Fever | – | + | ND |
| 20 | 41/M | None | 1 | NA | Fever, general fatigue | + | – | *S. pneumoniae** (*post-mortem* lung) |

Abbreviations: d: days, M: male, F: female, BMI: body mass index, +: positive, –: negative, CHF: chronic heart failure, COPD: chronic obstructive pulmonary disease, PCPS: percutaneous pulmonary support, ECMO: extracorporeal membrane oxygenation, NA: not applicable, VF: ventricular fibrillation, ND: not done, *S. pneumoniae*: *Streptococcus pneumoniae*, *P. aeruginosa*: *Pseudomonas aeruginosa*.
*Cultured during autopsy.

InfA-NP and for cell type-specific marker proteins, epithelial membrane antigen (EMA; epithelial cells), surfactant apoprotein D (SP-D; type II pneumocytes), cytokeratin AE1/AE3 (epithelial cells), CD68 (PG-M1; macrophages), and CD34 (endothelial cells), as previously described.[22] All mouse monoclonal antibodies, except for rabbit polyclonal antibody for SP-D, were purchased from DAKO Cytomation. Anti-SP-D antibody was purchased from Chemicon (Temecula, CA). Alexa Fluor 568-conjugated anti-mouse or anti-rabbit IgG (Molecular Probes, Eugene, OR), and Alexa Fluor 488-conjugated anti-rabbit or anti-mouse IgG (Molecular Probes) were used as secondary antibodies.

### Nucleic Acid Extraction and Real-Time RT-PCR (rRT-PCR) Assays

Nucleic acid extracts were prepared from the formalin-fixed and paraffin-embedded tissue sections (10 $\mu$m × 3) of 20 cases using a PureLink FFPE RNA total isolation kit (Invitrogen, Carlsbad, CA). The copy number of 2009 H1N1 was determined by rRT-PCR using an Mx3005P (Stratagene, La Jolla, CA) to amplify a segment within the hemagglutinin region of the 2009 H1N1 virus RNA. The amount of human $\beta$-actin mRNA in the DNase-treated RNA extracted from each section was also determined, and this internal reference gene was used to normalize the amount of RNA isolated from a specimen. To amplify 2009 H1N1-hemagglutinin region, forward (swH1N1-HA-F: 5′-CCCCATTGCA TTTGGGTAAA-3′) and reverse (swH1N1-HA-R: 5′-TGGAGAGTGATTCACACTCTGGAT-3′) primers were used with the labeled probe 5′-(FAM)AACATTG CTGGCTGGATCCTGGGA(TAMRA)-3′.[16] To amplify human $\beta$-actin mRNA, forward (5′-TGAGCGCGGCT ACAGCTT-3′) and reverse (5′-TCCTTAATGTCACG CACGATTT-3′) primers were used with the labeled probe 5′-(FAM)ACCACCACGGCCGAGCGG (TAMRA)-3′.[23] The copy numbers of 2009 H1N1-hemagglutinin/cell were calculated using the $\beta$-actin mRNA copy number, which was estimated to be 1500 copies/cell, as previously described.[16]

### Sequence Analysis of Hemagglutinin of the 2009 H1N1 Virus

Using the RNA samples extracted from viral antigen- and viral RNA-positive formalin-fixed and paraffin-embedded tissue sections, we analyzed the hemagglutinin sequence of the 2009 H1N1 virus. To determine amino acid substitution in the receptor binding site of the 2009 H1N1 virus, the hemagglutinin region (nt. 634–793) was amplified with QIAGEN OneStep RT-PCR (QIAGEN, Tokyo, Japan)

**Table 2** Histopathological findings in respiratory tracts of 20 autopsy cases

| *Histopathological features* | *Case number* | | | | | | | | | | | | | | | | | | | |
|---|---|---|---|---|---|---|---|---|---|---|---|---|---|---|---|---|---|---|---|---|
| | 1 | 2 | 3 | 4 | 5 | 6 | 7 | 8 | 9 | 10 | 11 | 12 | 13 | 14 | 15 | 16 | 17 | 18 | 19 | 20 |
| *Trachea, bronchus* | | | | | | | | | | | | | | | | | | | | |
| Desquamation of epithelium | 1+ | 3+ | 3+ | 1+ | 3+ | 3+ | 3+ | 2+ | 2+ | 1+ | 1+ | 2+ | 2+ | – | 2+ | 2+ | – | – | 1+ | – |
| Necrotizing tracheobronchitis | – | 2+ | – | – | 1+ | 1+ | 3+ | – | – | – | – | 1+ | – | – | 2+ | 1+ | – | – | – | – |
| Inflammatory cell infiltration | 1+ | 3+ | 1+ | 1+ | 1+ | 2+ | 3+ | 2+ | 2+ | – | 2+ | 3+ | 2+ | – | 2+ | 2+ | 1+ | – | 2+ | 2+ |
| Congestion | – | 2+ | 2+ | 3+ | 3+ | 2+ | 2+ | – | 3+ | 2+ | – | 1+ | 2+ | 1+ | – | 1+ | – | – | 3+ | 2+ |
| Hemorrhage | – | – | – | – | 1+ | 1+ | 1+ | 1+ | 1+ | – | – | 1+ | – | – | 1+ | – | – | – | 1+ | – |
| Submucosal gland inflammation | – | 3+ | 1+ | 1+ | 1+ | 1+ | 2+ | 1+ | 1+ | – | 1+ | 1+ | – | – | – | – | – | – | 1+ | 1+ |
| Mucosal eosinophilia | – | – | – | – | – | 1+ | – | 1+ | 2+ | 1+ | 1+ | 2+ | – | – | 3+ | – | – | – | – | – |
| *Bronchiole, alveolus* | | | | | | | | | | | | | | | | | | | | |
| Diffuse alveolar damage | 3+ | 3+ | 2+ | 2+ | – | – | – | – | – | – | 1+ | – | – | – | – | – | – | 3+ | – | – |
| Hyaline membrane formation | 2+ | 3+ | 3+ | 1+ | – | – | – | – | – | – | 1+ | – | – | – | – | – | – | – | – | – |
| Intra-alveolar edema | 2+ | 3+ | 3+ | 3+ | 3+ | 3+ | – | – | 1+ | – | | – | – | 2+ | – | – | 3+ | – | 3+ | 3+ |
| Intra-alveolar hemorrhage | 1+ | 1+ | – | 1+ | – | 2+ | – | – | 1+ | – | 2+ | 2+ | 2+ | 1+ | – | – | 3+ | 1+ | 2+ | 2+ |
| Congestion | 2+ | 1+ | 2+ | 3+ | 3+ | 3+ | – | – | 3+ | 1+ | – | – | – | 1+ | – | – | 1+ | – | 3+ | 3+ |
| Microthrombi | 1+ | – | – | – | – | – | – | – | – | – | 1+ | – | – | 1+ | – | – | – | 1+ | – | – |
| Inflammatory cell infiltration | 1+ | 3+ | 2+ | – | – | – | 1+ | 2+ | 1+ | – | 2+ | – | 2+ | – | – | – | 2+ | 1+ | – | – |
| Fibrosis | 1+ | 3+ | 1+ | 1+ | – | – | 2+ | 2+ | – | – | 2+ | 2+ | 1+ | 2+ | – | – | 3+ | 3+ | – | – |
| Type II cells hyperplasia | 3+ | – | – | – | – | – | – | – | – | – | 2+ | – | 1+ | 2+ | – | – | 2+ | 3+ | – | – |
| Bronchopneumonia with neutrophils | – | – | – | – | – | – | 3+ | 3+ | – | – | 1+ | – | 3+ | – | – | – | – | – | – | 2+ |
| *Others* | | | | | | | | | | | | | | | | | | | | |
| Heart failure cell | 3+ | 1+ | 1+ | 1+ | 2+ | – | – | – | 3+ | – | – | – | – | – | – | – | – | – | – | – |
| Emphysema | – | – | – | – | – | – | – | – | – | 3+ | – | – | – | 3+ | – | – | – | – | – | – |
| Plexiform pattern | – | – | – | – | – | – | – | – | – | – | 2+ | – | – | – | – | – | – | – | – | – |

No finding (–), mild (1+), moderate (2+), severe (3+).